공학박사 학위논문

Nanostructural Modification of Photoelectrode for the Highly Efficient Dye-Sensitized Solar Cells

광전극의 나노구조 변화를 통한 염료감응형태양전지 효율 향상

2013년 8월

서울대학교 대학원
재료공학부
남 창 우

Nanostructural Modification of Photoelectrode for the Highly Efficient Dye-Sensitized Solar Cells

광전극의 나노구조 변화를 통한 염료감응형태양전지 효율 향상

지도교수 박 병 우

이 논문을 공학박사 학위논문으로 제출함.
2013년 8월

서울대학교 대학원
재료공학부
남 창 우

남창우의 공학박사 학위논문을 인준함.

2013년 6월

위 원 장	강 신 후
부위원장	박 병 우
위 원	홍 성 현
위 원	고 민 재
위 원	이 현 정

Abstract

Dye-sensitized solar cell (DSSC) is an effective photoelectrochemical system that exhibits power-conversion efficiency over 10%. However, materials and systems of DSSC are almost optimized, so efficiency of device has been in stagnancy without a breakthrough for about 10 years. In addition, development of advanced technology is definitely needed for the mass production of device and thereby for the commercialization of DSSC. With these necessities, novel approaches have been attempted both in the research area and in the industrial area.

The main objective of my thesis is to develop novel photoelectrode materials for DSSC. To achieve the goal, I introduced the metal-induced nanostructures into the semiconducting TiO_2 film, so optical and nanostructural properties of photoelectrodes were manipulated. Unique optical properties of metal nanoparticles are utilized to enhance light absorption in photoelectrode and to improve the conversion efficiency of solar-cell device. Deposition of metal/semiconductor nanocomposites and subsequent selective etching of metal were conducted to obtain nanoporous thin-film photoelectrode. Optical and nanostructural properties of photoelectrodes were thoroughly investigated, and correlations to the photochemical properties of DSSCs were also made.

In Chapter 1, dye-sensitized solar cell (DSSC) is briefly reviewed. Operating principle, components, and materials for DSSC are explained. Particularly, various nanostructures for the photoelectrode of DSSC are introduced. Surface-plasmon

resonance in metal nanostructures is also concerned in this chapter, as a new strategy to improve light absorption and solar-cell properties.

In Chapter 2, gold nanoparticles of ~100 nm in diameter were incorporated into TiO_2 nanoparticles for dye-sensitized solar cells (DSSCs). At the optimum Au/TiO_2 mass ratio of 0.05, the power-conversion efficiency of the DSSC improved to 3.3% from a value of 2.7% without Au, and this improvement was mainly attributed to the photocurrent density. The Au nanoparticles embedded in the nanoparticulate-TiO_2 film strongly absorbed light due to the localized surface-plasmon resonance, and thereby promoted light absorption of the dye. In the DSSCs, the 100 nm-diameter Au nanoparticles generate field enhancement by surface-plasmon resonance rather than prolonged optical paths by light scattering.

In Chapter 3, a facile method to synthesize nanoporous-TiO_2 thin film for dye-sensitized solar cell (DSSC) was introduced. Silver/TiO_2 co-sputtering led to the formation of nanocomposite film which consists of silver nanoclusters and surrounding TiO_2 matrix, and subsequently, Ag nanoclusters in nanocomposite were selectively etched by just immersing in nitric acid. Nanoporous-TiO_2 DSSC fabricated by this simple and straightforward process showed the power-conversion efficiency of 3.4% under 1 sun condition, at the thickness of only 1.8 μm.

Keywords: dye-sensitized solar cell, surface plasmon, nanoporous, sputtering, solar cell, titanium dioxide

Student Number: 2009-30150

Table of Contents

List of Figures

Chapter 1.

Chapter 2.

Chapter 3.

List of Table

Chapter 3.

Chapter 1. Overview

1.1. Introduction to Dye-Sensitized Solar Cells

In 1991, Professor Michael Grätzel introduced photoelectrochemical cells exhibited power conversion efficiency of ~8% [1]. The most remarkable feature of this cell compared with the conventional semiconductor solar-cell systems is that the role of light absorption and photocarrier transport is separated. Photosensitive dyes absorb light and transfer generated photoelectrons to the conduction band of semiconductor, and the photoelectrons diffuse through semiconductor and finally make a photovoltaic effect. Introduction of nanostructured semiconductor led to the high photocurrent and superior power-conversion efficiency, since it allowed about 3 orders larger surface area than the projected one so according large amount of dye were adsorbed on the semiconductor. This kind of solar cell is called as dye-sensitized solar cell (DSSC), and has been actively investigated for over 20 years.

Constitution of typical DSSC is depicted in Fig. 1-1. Dyes are chemisorbed on surface of semiconductor, and the thickness of the dye-adsorbed nanoparticulate semiconductor layer is several micrometers. To complete the circuit, electron should be supplied to photooxidized dye, so redox species in electrolyte is needed for electron transfer. The redox species which transfer electrons to oxidized dyes are reduced at counter electrode. Redox species repeat oxidation and reduction in cell to operate DSSC normally. Electrode material of DSSC should both be transparent in visible range to pass the light to the photoactive region, and be electrically conductive to transfer

photocurrent to external circuit. Transparent conducting oxide (TCO) satisfies both two conditions, so DSSC use TCO films as electrode materials.

The basic electron transfer processes in a DSSC, as well as the electrical potentials of typical DSSC at open-circuit condition are shown in Fig. 1-2 [2]. In this schematic diagram, materials for dye, semiconductor, and redox couple are ruthenium-based N3 dye, titanium dioxide (TiO_2), and I^-/I_3^-, respectively. Electrons in dye are excited by photon (process 0), and subsequently these excited electrons are injected into the conduction band of a semiconductor film (process 2). Injected electrons move toward TCO contact by diffusion (process 4), and flow to external load to generate electrical work. Triiodide ions (I_3^-) in electrolyte are reduced by electron transfer at counter electrode (process 7), and oxidized dyes are regenerated by electron donation from redox couple (process 3). Besides the desired pathway of the electron transfer processes (processes 2, 3, 4, and 7) described above, the loss reactions are also indicated (processes 1, 5, and 6). Reaction 1 is direct recombination of the excited dye reflected by the excited state lifetime. Recombination of injected electrons in the TiO_2 with either oxidized dyes or acceptors in the electrolyte is numbered as 5 and 6, respectively. In principle, electron transfer to I_3^- can occur either at the interface between the nanocrystalline oxide and the electrolyte or at areas of the TCO that are exposed to the electrolyte.

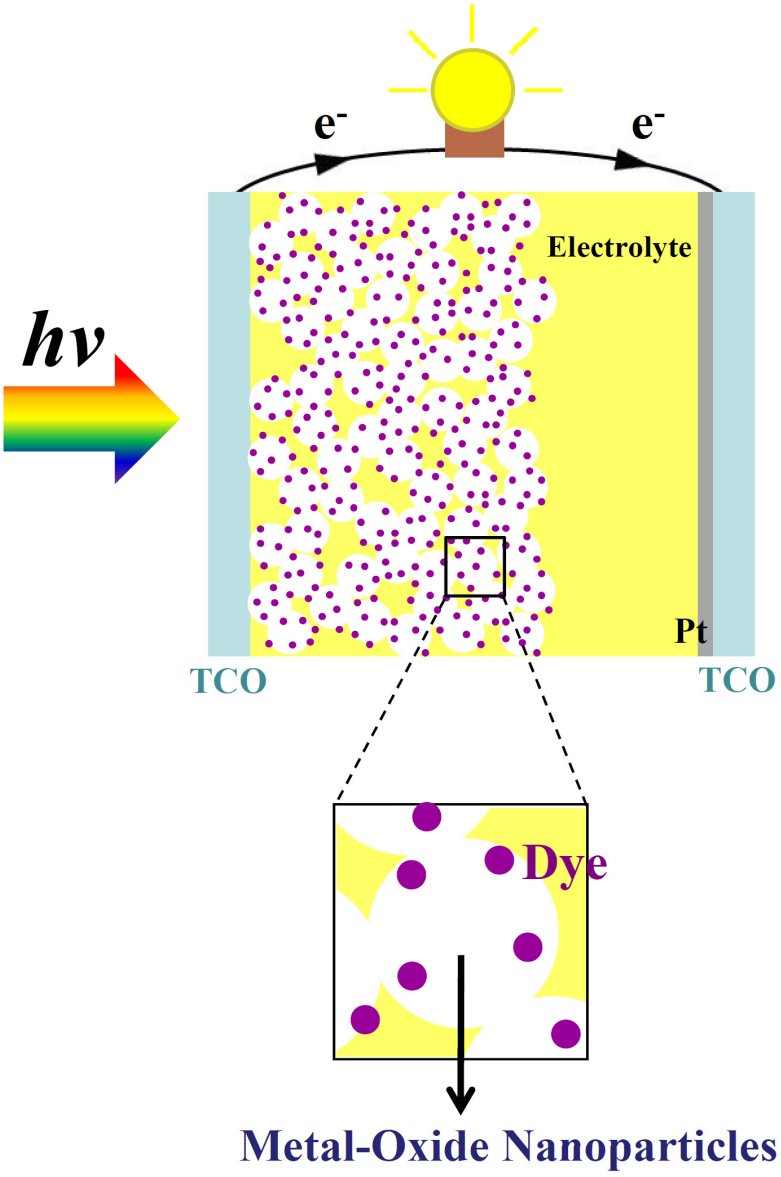

Fig. 1-1. (Color) Schematic figure representing a composition of dye-sensitized solar cell (DSSC) and photoelectron flow in DSSC.

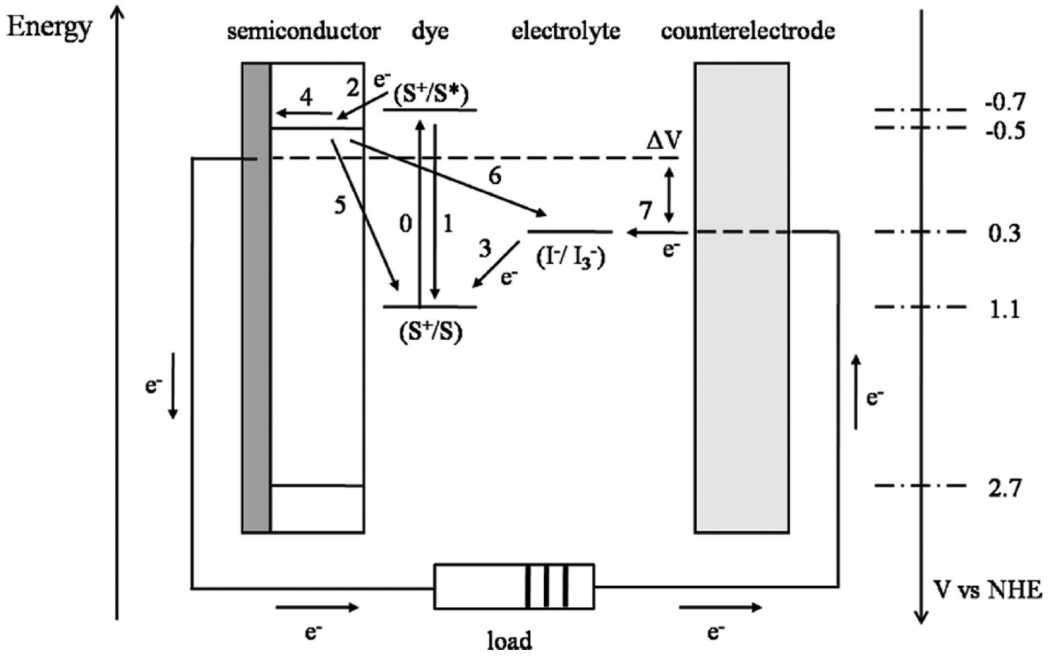

Fig. 1-2. Simple energy level diagram for DSSC. The basic electron transfer processes are indicated by numbers (1-7). From Ref. [2].

1.2. Materials in Dye-Sensitized Solar Cells

Dye is the most important component of DSSC, since it determines the performances of overall device. Energy level difference between the lowest unoccupied molecular orbital (LUMO) and the highest occupied molecular orbital (HOMO) of dye sets the wavelength-range of light that DSSC can absorb. Particularly, ruthenium-complex dyes have been found to be an outstanding light absorber and charge-transfer sensitizer, with excellent stability (Fig. 1-3) [3]. DSSC sensitized with ruthenium-based N719 dye exhibits power-conversion efficiency about 10%. Recently, porphyrin molecule is engineered and applied to DSSC as sensitizing material, and shows power-conversion efficiency of 12.3% in device, which is the highest value observed in DSSC system (Fig. 1-4) [4].

The main role of semiconductor material in DSSC is conduction of photoelectron. In addition, conduction band of semiconductor should lie on proper position both for easy injection of photoelectron from dye and for higher open-circuit voltage. Metal-oxide semiconductor is widely used for DSSC due to their superior electron-transport property, suitable band structure, and higher stability. Among the various metal-oxide materials, titanium dioxide (TiO_2) shows the best properties, so high-efficiency DSSCs exhibiting power-conversion efficiency over 10% are made of TiO_2 photoelectrode [5]. Typical photoelectrode of DSSC consisting of connecting TiO_2 nanoparticles is shown in Fig. 1-5.

Tin-doped indium oxide, also known as ITO, has both superior electrical conductivity and higher optical transmittance in visible region, but rarely used for DSSC since ITO film is thermally unstable [6]. Photoelectrode of DSSC is annealed at about

500°C to enhance connectivity of nanocrystalline TiO_2, so TCO film should have a thermal stability at according temperature. Since fluorine-doped tin oxide (FTO) is stable at 500°C and has moderate optical and electrical properties, photoelectrode of DSSC is fabricated on FTO-coated glass in most cases.

With regards to the hole-conducting medium, electrolytes based on the I^-/I_3^- redox couple have been the preferred choice [2]. Nitrile-based liquid solvents give the highest efficiencies, whereas gelification of the solvent or ionic liquids is used for the best stability, compromising somewhat the efficiency. Successful results have also been achieved with other redox systems such as cobalt-based systems, $SCN^-/(SCN)_3^-$, and various organic systems.

Counter electrode for DSSC with I^-/I_3^- electrolytes can be prepared by deposition of a thin catalytic layer of platinum onto a FTO substrate. Without platinum, FTO is a very poor counter electrode and has a very high charge-transfer resistance, more than 10^6 Ω cm^2, in a standard I^-/I_3^- electrolyte [7]. Charge-transfer resistances of less than 1 Ω cm^2 and consequent normal operation of DSSC can be achieved with very low Pt-loadings (5 μg cm^{-2}). The most common counter electrode for DSSC is a platinized conducting glass, but also carbon materials and conducting polymers have been developed.

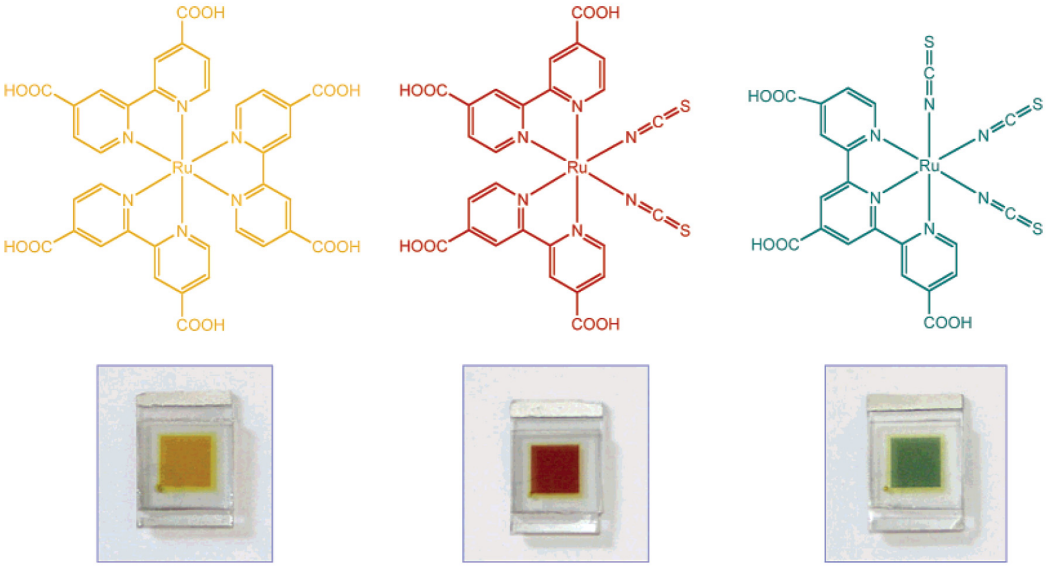

Fig. 1-3. (Color) Molecular structure of three ruthenium-based dye for DSSC. The lower part of the figure shows nanocrystalline TiO_2 films loaded with the respective sensitizer. From Ref. [3].

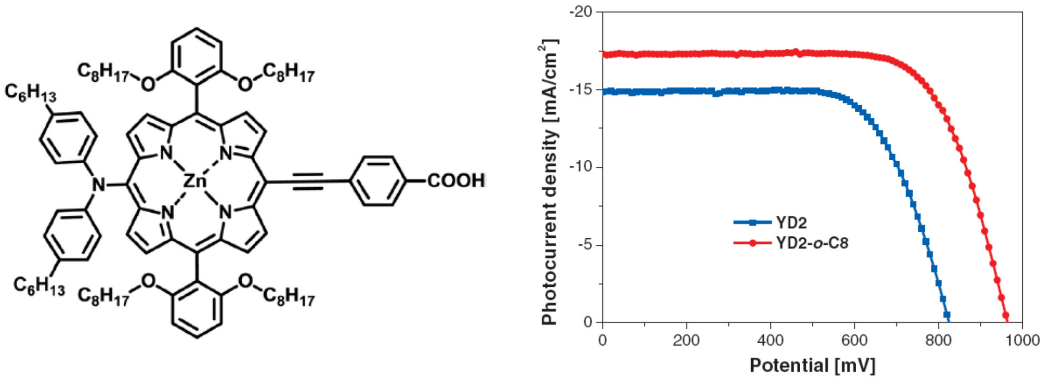

Fig. 1-4. (Color) Molecular structure of zinc porphyrin dye as sensitizer of DSSC (left). Current density-voltage (*J*-*V*) curve shows power conversion efficiency of 12.3% with this sensitizer (right). From Ref. [4].

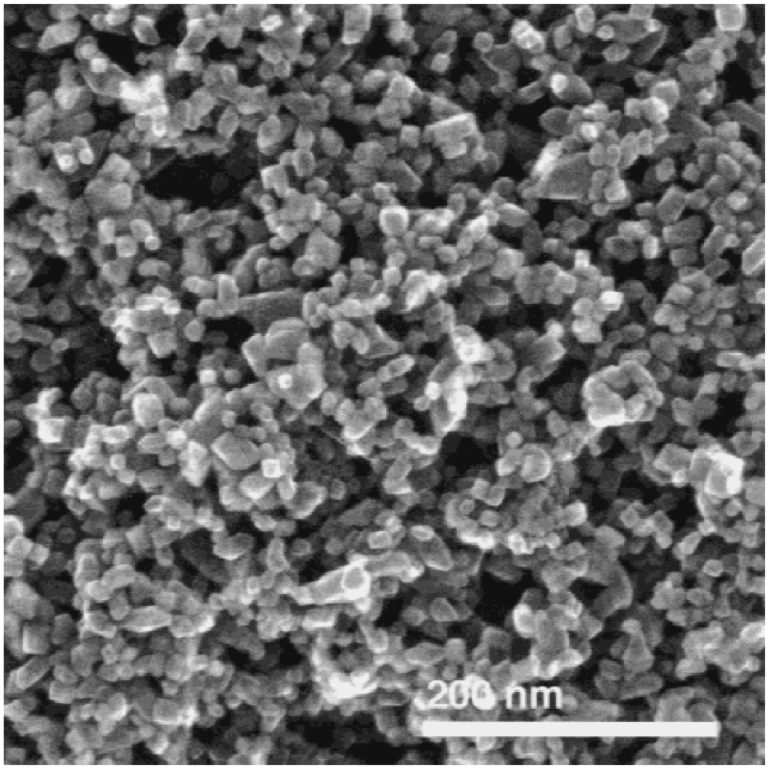

Fig. 1-5. Electron microscopic image of TiO_2 nanoparticulate film for photoelectrode of DSSC. From Ref. [5].

1.3. Nanostructured Photoelectrodes

The key to the breakthrough for DSSC was the introduction of a nanoparticulate-TiO_2 electrode with a high internal surface area, to support the monolayer of a sensitizing molecule. The most common technique for preparation of TiO_2 nanoparticles is the hydrolysis of a titanium precursor followed by hydrothermal growth and crystallization [5]. The synthesized colloidal nanoparticles are formulated in a paste with polymer additives and deposited onto FTO-glass substrate with doctor-blade or screen-printing techniques. Finally, the film is sintered at about 500°C in air to remove organic components and to make electrical connection between the nanoparticles. The diameter of synthesized nanoparticles for DSSC is about 20 nm, and the resultant film has the porosity of ~60% [8].

During the last years, large efforts have been paid to optimize the morphology of the nanostructured photoelectrode of DSSC. Various nanostructures, such as random assemblies of nanoparticles, arrays of nanotubes, and single-crystalline nanorods, have been applied as photoelectrode of DSSC with motivations of improving charge transport and enhancing pore filling of hole-conductor materials.

Ordered arrays of vertically oriented TiO_2 nanotubes can be grown by potentiostatic anodization in fluoride-based electrolytes [9-11]. TiO_2 nanotubes are typically grown using Ti foil, but growth can also be obtained from Ti thin films deposited on FTO-coated glass. The length of the nanotubes, wall thickness (5-34 nm), pore diameter (12-240 nm), and tube-to-tube spacing (0-10 nm) can be controlled by the experimental conditions. A TiO_2 nanotube-based DSSC on Ti substrate achieved power-

conversion efficiency of 6.9% [10], and nanotubes grown on a FTO substrate with the thickness of 1.1 μm showed efficiency of 4.1% [11]. Electron microscopic image of TiO_2 nanotubes is shown in Fig. 1-6.

TiO_2-nanorods based photoelectrode exhibited about 10-fold higher electron diffusivity compared with the typical nanoparticulate-TiO_2 film, but showed lower power-conversion efficiency in solar-cell device [12]. It is due to the low surface area of photoelectrode and thereby less amount of adsorbed dye on device. To resolve this problem, advanced nanostructures such as nanotree have been suggested. Secondary braches were grown on the primary single-crystalline nanorods, as shown in Fig. 1-7, so the solar-cell efficiency was enhanced as the surface area of photoelectrode increased [13].

Other novel nanostructures for DSSC-photoelectrode have been studied. Metal-oxide aggregates composed of 20 nm-sized nanoparticles have large surface area for the highly efficient device, as well as light scattering properties coming from the size of aggregates with several hundred nanometer [14]. TiO_2 photonic-crystal film is expected to exhibit higher solar-cell performances due to their strong light-trapping properties, caused by periodic arrangement of submicron-sized pores (Fig. 1-8) [15].

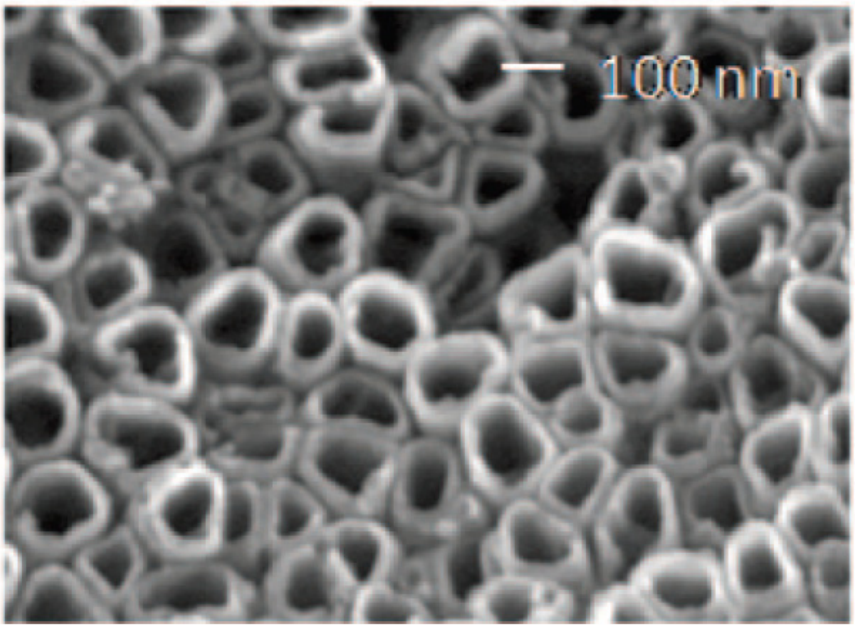

Fig. 1-6. Scanning electron microscopy image (top view) of TiO_2 nanotubes. From Ref. [9].

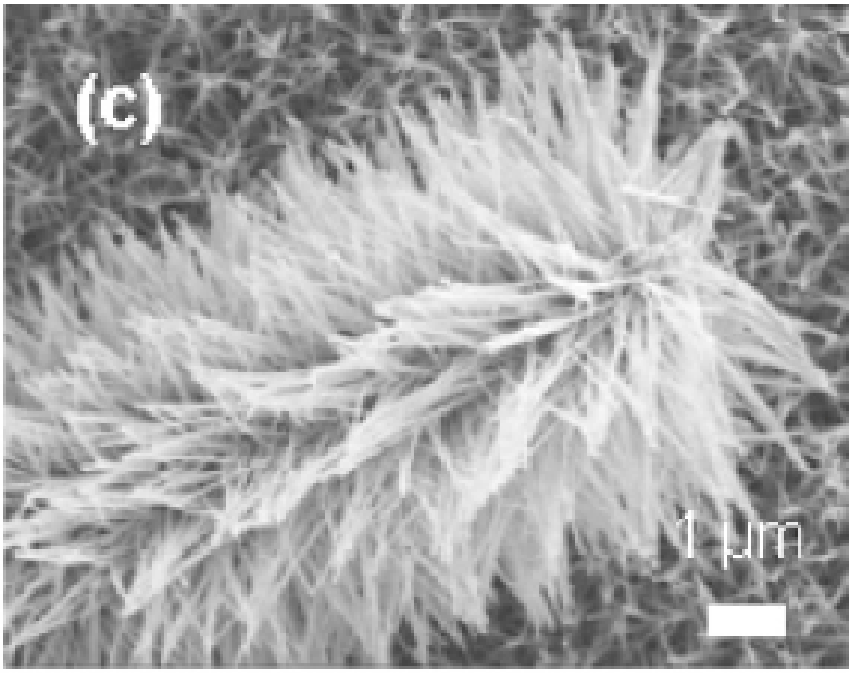

Fig. 1-7. ZnO nanotree-shape photoelectrode for DSSC. From Ref. [13].

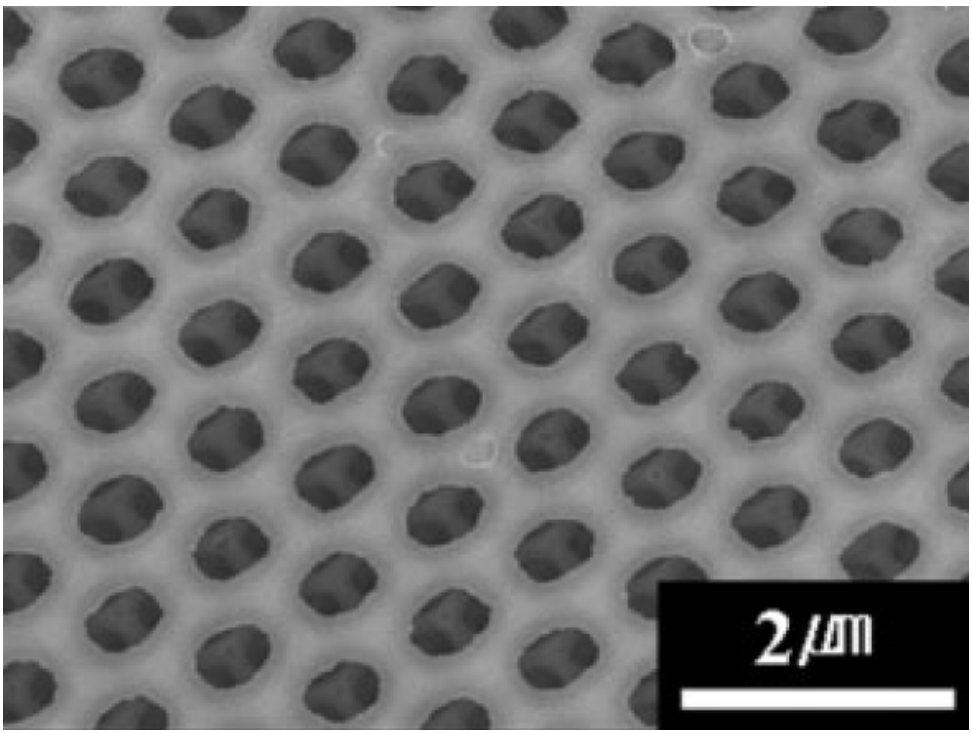

Fig. 1-8. Electron microscopic image of TiO_2 film with periodic pores. From Ref. [15].

1.4. Surface-Plasmon Resonance in Metal Nanostructures

The optical properties of metal nanostructures are clearly different from bulk materials due to resonance in the collective motion of free electrons oscillating within a small geometric range, and this collective electron oscillation induced by electromagnetic wave is called surface-plasmon resonance [16]. Schematic drawing of the interaction of an electromagnetic radiation with metal nanostructures is depicted in Fig. 1-9. The electric field of the incoming radiation induces the formation of a dipole in the nanoparticle, and there is a restoring force that tries to compensate it, so that a unique resonance frequency matches this electron oscillation within the nanoparticle. For nonspherical particles, such as rods, the resonance wavelength depends on the orientation of the electric field relative to the particle, and thus, oscillations either longitudinal or transversal are possible.

The optical properties of metal nanoparticles are clearly different from bulk materials due to surface plasmon. As shown in the inset of Fig. 1-10, Au-nanoparticle solutions indicate various colors in accordance with the size of nanoparticle, and all of these colloids do not show unique luster observed in bulk gold [16]. Absorbance peaks of Au nanoparticles are appeared between 500 nm and 600 nm, which mean that Au nanoparticles strongly interact with light of this wavelength region. Metal nanostructures strongly interact with photons which have similar energy with their plasmon-resonance energy. For example, an aluminum nanoparticle of 13 nm diameter has surface-plasmon resonance energy of ~8.8 eV, and its absorption efficiency for light of energy 8.8 eV is 18 [17], which means that cross section area for absorption is 18 times

greater than its geometrical cross section. Field lines of the Poynting vector visualize the photon paths (Fig. 1-11). Strong convergence of field lines near the nanoparticle indicates that light passing near the metal deflects toward it, and that is, light is strongly absorbed by the nanoparticle.

When surface plasmon is excited, electromagnetic field in the vicinity of metal nanostructures is strongly amplified. The enhancement factor η (intensity ratio of the resultant to incident field) can be calculated assuming one isotropic metal sphere is placed in a homogeneous medium [18]:

$$\eta = \frac{\left|\vec{E}_2\right|^2}{\left|\vec{E}_0\right|^2} = \left(\left| 1 + 2\frac{a^3}{r^3}\frac{\varepsilon_{metal} - \varepsilon_{medium}}{\varepsilon_{metal} + 2\varepsilon_{medium}} \right|^2 \cos^2\theta + \left| -1 + \frac{a^3}{r^3}\frac{\varepsilon_{metal} - \varepsilon_{medium}}{\varepsilon_{metal} + 2\varepsilon_{medium}} \right|^2 \sin^2\theta \right).$$

where ε_{metal} and ε_{medium} are the dielectric constants of the metal nanoparticle and the surrounding medium, respectively, and a and r are the radius of the metal nanoparticle and the distance from the center of the metal nanoparticle, respectively. Figure 1-12 shows the field enhancement near the Au nanoparticle at the wavelength of 550 nm. Field enhancement leads to the enhancement of light absorption near the metal nanostructures, and thereby creation of photocarriers in the surrounding semiconductor is facilitated [19]. As shown in Fig. 1-13, dye-adsorbed TiO_2 photoelectrode absorbs more light when silver nanoparticles are contained in the electrode [20]. This field-enhancement effect can be effectively utilized for light harvesting in solar-cell devices.

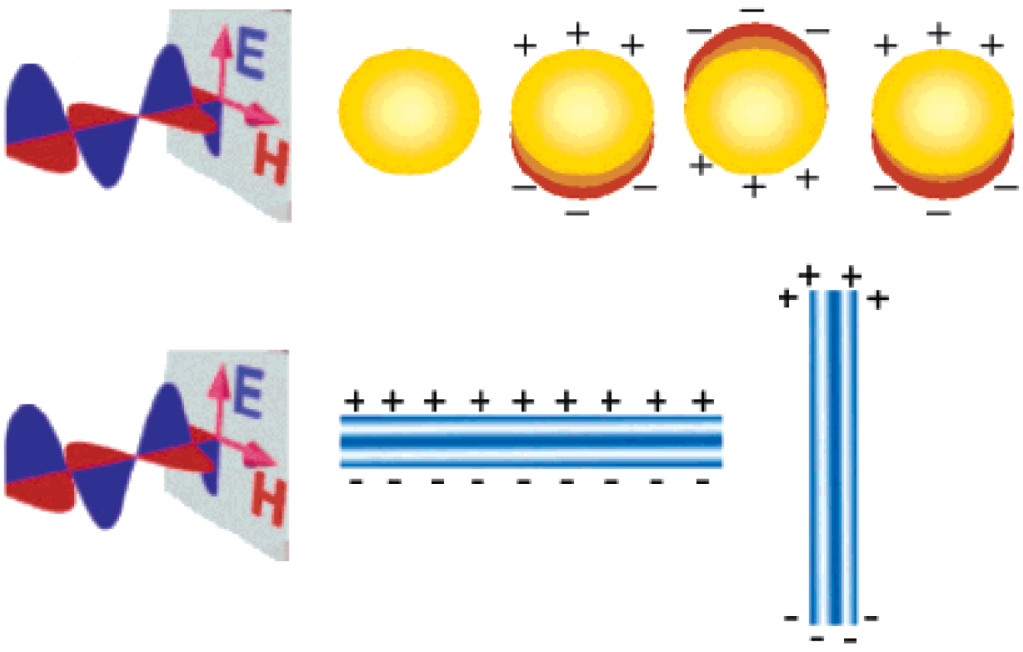

Fig. 1-9. (Color) Schematic figure showing an excitation of surface plasmon in metal nanostructures by electromagnetic radiation. From Ref. [16].

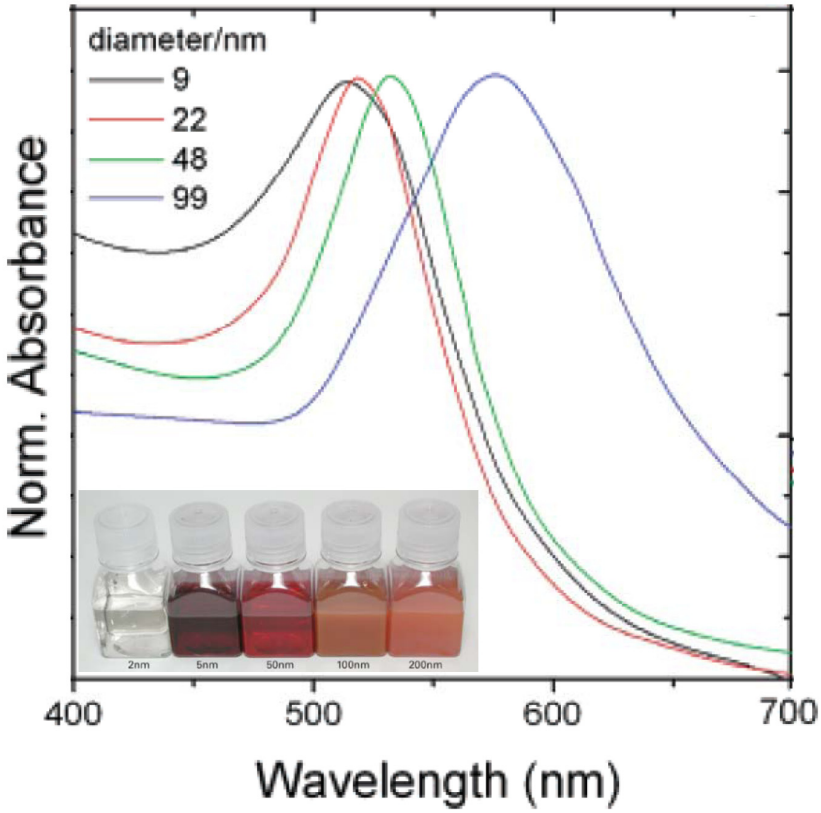

Fig. 1-10. (Color) UV-visible extinction spectra of gold-nanoparticle colloid with various size. Inset shows a picture of diverse colloidal Au varied with nanoparticle size. From Ref. [16].

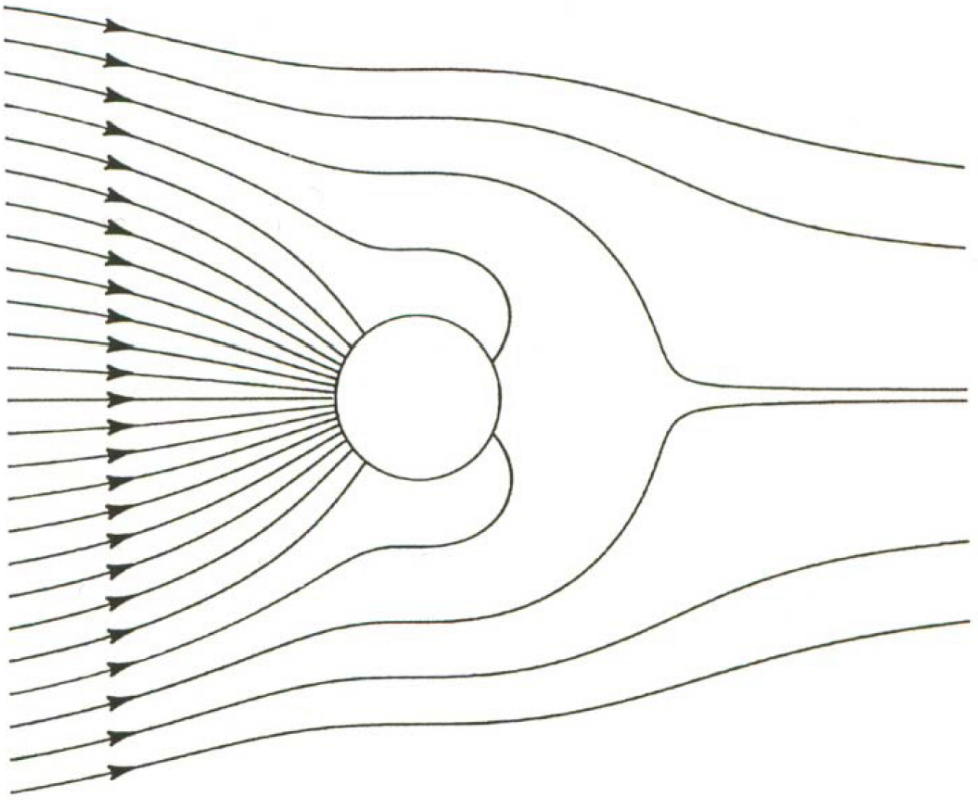

Fig. 1-11. Field lines of the total Poynting vector around an aluminum nanoparticle illuminated by 8.8 eV photon, which is the surface-plasmon resonance energy of aluminum nanoparticle. From Ref. [17].

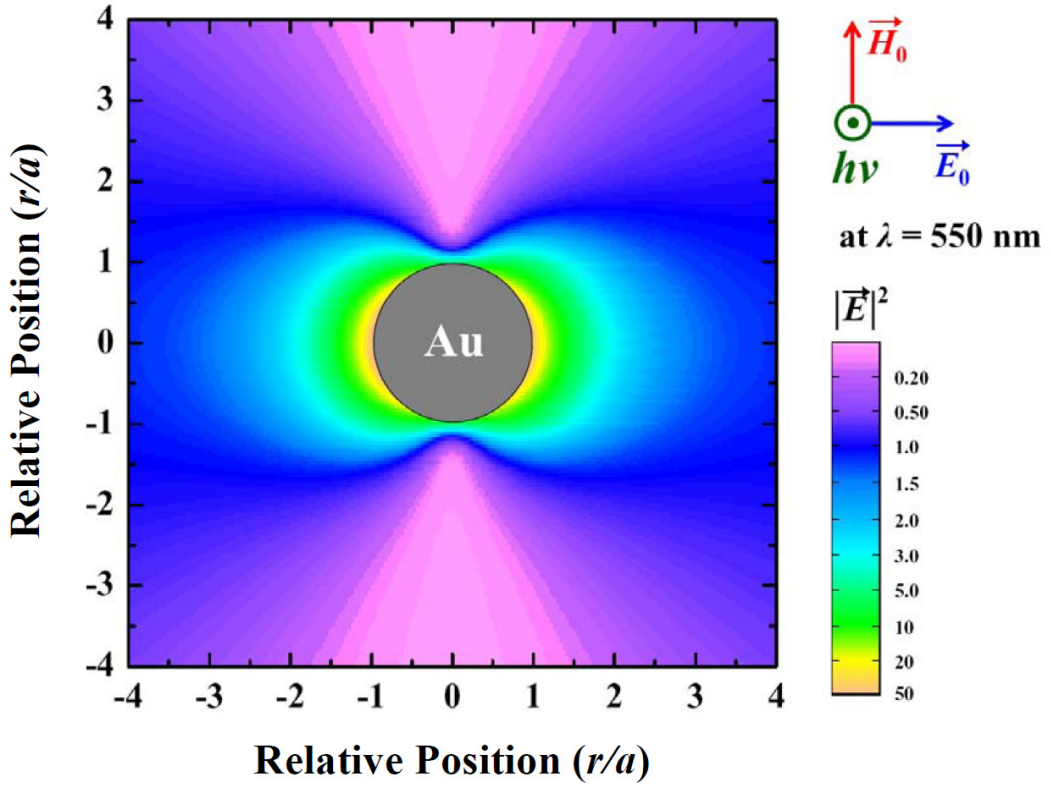

Fig. 1-12. (Color) Calculated field-enhancement factor of Au nanoparticle. The dielectric constants of metal and surrounding medium are -5.181 + 2.094·*i* and 2.220 + 0·*i*, respectively.

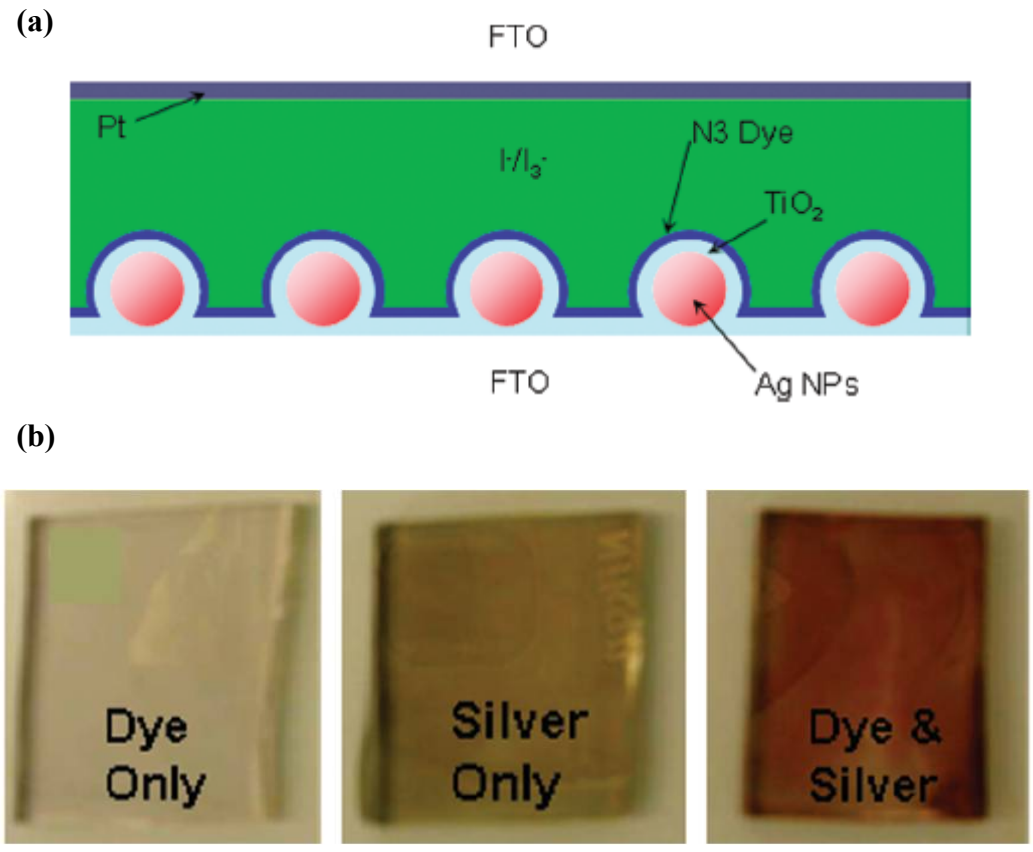

Fig. 1-13. (Color) (a) Configuration of solar cells containing silver nanoparticles and dye, and (b) photos of anodes showing the enhancement of light absorption by the introduction of Ag. From Ref. [20].

1.5. Objective of Research

The main objective of this study is to develop novel photoelectrode materials for DSSC, with the merits of either the higher efficiency or the advanced fabrication method. To achieve the goal, I introduced the metal-induced nanostructures into the semiconducting TiO_2 film.

Improving power-conversion efficiency of device is the ultimate goal of solar-cell research. In DSSC, however, materials and systems are almost optimized, so efficiency of device has been in stagnancy without a breakthrough for about 10 years. Recently, new concepts have been applied to DSSC, and among these, one of the attractive topic is a surface-plasmon resonance arising in metal nanostructures. In this research, gold nanoparticles with a diameter of 100 nm were inserted into the nanoparticulate-TiO_2 photoelectrode, to study the plasmonic effects on optical properties of photoelectrode and finally to improve the solar-cell efficiency of DSSC.

To commercialize and industrialize DSSC module (Fig. 1-14), technologies both for large-area deposition and mass production of photoelectrode are necessary. However, screen printing and doctor-blade method, which are conventionally used to fabricated the photoelectrode of DSSC, do not satisfy those needs. Sputtering is a powerful method for thin-film deposition which guarantees the high uniformity and reproducibility in large area, but compact film structure resulted from sputtering method is not suitable for the photoelectrode of DSSC. To fabricate nanoporous-TiO_2 thin films with sputtering method, silver/TiO_2 nanocomposite thin films were deposited and subsequently the silver nanoclusters in films were selectively etched. Nanostructural, optical, and

photoelechemical properties of films were thoroughly investigated to examine the availability of this simple two-step process.

Fig. 1-14. (Color) Building-integrated DSSC demonstrator from Dyesol. From Ref. [2].

1.6. References

1. B. O'Regan and M. Grätzel, "A Low-Cost, High-Efficiency Solar Cell Based on Dye-Sensitized Colloidal TiO_2 Films, " *Nature* **353**, 737 (1991).
2. A. Hagfeldt, G. Boschloo, L. Sun, L. Kloo, and H. Pettersson, "Dye-Sensitized Solar Cells," *Chem. Rev.* **110***,* 6595 (2010).
3. M. Grätzel, "Solar Energy Conversion by Dye-Sensitized Photovoltaic Cells," *Inorg. Chem.* **44**, 6841 (2005).
4. A. Yella, H.-W. Lee, H. N. Tsao, C. Yi, A. K. Chandiran, M. K. Nazeeruddin, E. W.-G. Diau, C.-Y. Yeh, S. M. Zakeerudding, and M. Grätzel, "Porphyrin-Sensitized Solar Cells with Cobalt (II/III)-Based Redox Electrolyte Exceed 12 Percent Efficiency," *Science* **334**, 629 (2011).
5. C. J. Barbé, F. Arendse, P. Comte, M. Jirousek, F. Lenzmann, V. Shklover, and M. Grätzel, "Nanocrystalline Titanium Oxide Electrodes for Photovoltaic Applications," *J. Am. Ceram. Soc.* **80**, 3157 (1997).
6. B. Yoo, K. Kim, S. H. Lee, W. M. Kim, and N.-G. Park, "ITO/ATO/TiO_2 Triple-Layered Transparent Conducting Substrates for Dye-Sensitized Solar Cells," *Sol. Energy Mater. Sol. Cells* **92**, 873 (2008).
7. A. Hauch and A. Georg, "Diffusion in the Electrolyte and Charge-Transfer Reaction at the Platinum Electrode in Dye-Sensitized Solar Cells," *Electrochim. Acta* **46**, 3457 (2001).
8. P. Wang, S. M. Zakeeruddin, P. Comte, R. Charvet, R. Humphry-Baker, and M.

Grätzel, “Enhance the Performance of Dye-Sensitized Solar Cells by co-Grafting Amphiphilic Sensitizer and Hexadecylmalonic Acid on TiO_2 Nanocrystals,” *J. Phys. Chem. B* **107**, 14336 (2003).

9. G. K. Mor, O. K. Varghese, M Paulose, K. Shankar, and C. A. Grimes, “A Review on Highly Ordered, Vertically Oriented TiO_2 Nanotube Arrays: Fabrication, Material Properties, and Solar Energy Applications,” *Sol. Energy Mater. Sol. Cells* **90**, 2011 (2006).
10. K. Shankar, G. K. Mor, H. E. Prakasam, S. Yoriya, M. Paulose, O. K. Varghese, and C. A. Grimes, “Highly-Ordered TiO_2 Nanotube Arrays up to 220 μm in Length: Use in Water Photoelectrolysis and Dye-Sensitized Solar Cells,” *Nanotechnology* **18**, 065707 (2007).
11. K. Shankar, J. Bandara, M. Paulose, H. Wietasch, O. K. Varghese, G. K. Mor, T. J. LaTempa, M. Thelakkat, and C. A. Grimes, “Highly Efficient Solar Cells Using TiO_2 Nanotube Arrays Sensitized with a Donor-Antenna Dye,” *Nano Lett.* **8**, 1654 (2008).
12. C.-H. Ku and J.-J. Wu, “Electron Transport Properties in ZnO Nanowire Array/Nanoparticle Composite Dye-Sensitized Solar Cells,” *Appl. Phys. Lett.* **91**, 093117 (2007).
13. S. H. Ko, D. Lee, H. W. Kang, K. H. Nam, J. Y. Yeo, S. J. Hong, C. P. Grigoropoulos, and H. J. Sung, “Nanoforest of Hydrothermally Grown Hierarchical ZnO Nanowires for a High Efficiency Dye-Sensitized Solar Cell,” *Nano Lett.* **11**, 666 (2011).

14. Q. Zhang, T. P. Chou, B. Russo, S. A. Jenekhe, and G. Cao, "Aggregation of ZnO nanocrystallites for High Conversion Efficiency in Dye-Sensitized Solar Cells," *Angew. Chem. Int. Ed.* **47**, 2402 (2008).
15. E. S. Kwak, W. Lee, N.-G. Park, J. Kim, and H. Lee, "Compact Inverse-Opal Electrode Using Non-Aggregated TiO2 Nanoparticles for Dye-Sensitized Solar Cells," *Adv. Funct. Mater.* **19**, 1093 (2009).
16. L. M. Liz-Marzan, "Tailoring Surface Plasmons through the Morphology and Assembly of Metal Nanoparticles," *Langmuir* **22**, 32 (2006).
17. C. F. Bohren and D. R. Huffman, *Absorption and Scattering of Light by Small Particles*, p. 340, Wiley, New York (1983).
18. K. Tanabe, "Field Enhancement around Metal Nanoparticles and Nanoshells: a Systematic Investigation," *J. Phys. Chem. C* **112**, 15721 (2008).
19. H. A. Atwater and A. Polman, "Plasmonics for Improved Photovoltaic Devices," *Nat. Mater.* **9**, 205 (2010).
20. S. D. Standridge, G. C. Schatz, and J. T. Hupp, "Distance Dependence of Plasmon-Enhanced Photocurrent in Dye-Sensitized Solar Cells," *J. Am. Chem. Soc.* **131**, 8407 (2009).

Chapter 2.

The Effects of 100 nm-Diameter Au Nanoparticles on Dye-Sensitized Solar Cells

2.1. Introduction

The optical properties of metal nanoparticles are clearly different from bulk materials due to resonance in the collective motion of free electrons oscillating within a small sphere [1], and this collective electron oscillation induced by electromagnetic wave is called surface-plasmon resonance. As the plasmonic resonance induces a dipole on the metal nanoparticle, the electric field is enhanced around the metal nanoparticle, and the optical extinction, such as scattering and absorption, is intensified [2]. In particular, it is explained that the electric-field enhancement is the origin of the fluorescence enhancement induced by metal nanostructures [3] and the surface enhanced Raman scattering (SERS) [4]. The plasmonic resonance of gold and silver nanoparticles has been intensively studied because they strongly interact with visible light, and it has been applied on a wide scale with chemical sensing [5], Raman spectroscopy [6], photoluminescence enhancement [7], etc.

The work presented in Chapter 2 was published in *Appl. Phys. Lett.* **99**, 253107 (2011) entitled, "The Effects of 100 nm-Diameter Au Nanoparticles on Dye-Sensitized Solar Cells."
Changwoo Nahm, Hongsik Choi, Jongmin Kim, Dae-Ryong Jung, Chohui Kim, Joonhee Moon, Byungjoo Lee, and Byungwoo Park*

In a solar cell system, it is important that the active layer of the solar cell absorbs as many photons as possible to produce more carrier electrons. In other words, the same photocurrent may be produced with a reduced film thickness, and additional enhancement is also expected in thinner solar cells owing to the suppressed carrier recombination and therefore decreased internal resistance. Metal nanoparticles can contribute to the effective light absorption of solar cells, both by local field enhancement through the localized surface-plasmon resonance and by light scattering leading to prolonged optical-path lengths [8].

The enhanced photovoltaic properties from the incorporation of metal nanoparticles have been studied for various systems [9-12]. More recently, metal nanoparticles were also introduced to the electrodes of dye-sensitized solar cells (DSSCs), and the solar-cell properties were improved by the plasmon-enhanced absorption of the dyes [13-16]. However, the size of the metal nanoparticles used in the previous studies for DSSCs was limited to 10 - 30 nm, and the effects of larger metal nanoparticles on DSSCs have not been investigated yet.

Many researchers demonstrated that the size of the metal nanoparticles is a key factor for determining the plasmonic phenomena, and especially, light scattering occurs more dominantly than light absorption as the size of the metal nanoparticles increases [2,17]. Nevertheless, in this article, we report that the Au nanoparticles with 100 nm diameters can improve the photovoltaic efficiency of DSSCs mainly by the localized surface-plasmon resonance, not by light scattering.

2.2. Experimental Section

Gold nanoparticles were synthesized by reduction of Au ions in aqueous solution [18], and concentrated Au colloid were mixed with commercial TiO_2 nanopowders (P25: Degussa, average diameter of 25 nm) to make a paste for the photoelectrode of DSSCs. Commercial N719 dye (Solaronix) was used as sensitizer, and sandwich-type DSSCs were fabricated [19].

Commercial TiO_2 nanopowders, instead of TiO_2 pastes from Solaronix® or Dyesol®, were used for mixing with ~100 nm Au nanoparticles and for better reproducibility of experiments. In addition, thinner TiO_2 films (4 μm) than the typical thicknesses of DSSCs (~10 μm) were employed to clarify the effects caused by metal nanoparticles. These factors led to the lower power-conversion efficiency of 2.7% for the bare DSSC, compared with typical DSSCs exhibiting over 5% [19].

Synthesis of Au Nanoparticles: Gold nanoparticles were synthesized by the reduction of gold chloride trihydrate ($HAuCl_4 \cdot 3H_2O$; Aldrich) [18]. As a 0.5 mM aqueous solution of gold chloride trihydrate was stirred, ascorbic acid solution was added as a reducing agent. The resulting Au nanoparticle solution was concentrated by repeated centrifugation, and the contents of Au were varied (7 mg, 21 mg, 35 mg, and 49 mg) while the volume of the concentrated Au solution was fixed at 4.9 *mL*.

Preparation of Au/TiO_2 Mixture Pastes: Commercial TiO_2 nanopowders (P25: Degussa, average diameter of 25 nm) were used as the electrode material of DSSCs. Acid-treated TiO_2 powders [20,21] (0.7 g) were added to the concentrated Au solution (4.9 *mL*), and

both polyethylene glycol (0.14 g, Fluka, average MW 20,000) and polyethylene oxide (0.14 g, Alfa Aesar, average MW 100,000) were added to the Au/TiO_2 mixture solution for the viscous paste [22,23]. Mixture pastes of various Au/TiO_2 mass ratios (0, 0.01, 0.03, 0.05, and 0.07) were prepared simultaneously, and these mixtures were stirred for a day to yield the homogeneous paste.

Fabrication of Dye-Sensitized Solar Cells (DSSCs): For fabricating the nanoparticulate-TiO_2 films that were 4 μm thick, the resulting pastes were coated on a fluorine-doped tin oxide substrate (FTO, TEC 8: Pilkington) by a simple doctor-blade method [23,24]. A strip of Scotch Magic Tape (3M) was punched to make a mold for doctor blade and to fix the active area of DSSCs as 0.28 cm^2. After annealing at 500°C for 30 min, the paste-coated electrodes were immersed in 0.3 mM anhydrous ethanol solution of N719 dye ($RuL_2(NCS)_2$:2TBA, L = 2,2′-bipyridyl-4,4′-dicarboxylic acid, TBA = tetrabutylammonium; Solaronix) for 12 h at room temperature. The dye-adsorbed electrode and Pt thin film for the counter electrode were sealed with thermoplastic foil (Dupont, nominal thickness 60 μm), and an iodide-based redox electrolyte (AN-50: Solaronix) was injected into the gap between the two electrodes.

Characterization: Field-emission scanning electron microscopy (FE-SEM, SU70: Hitachi) was used to investigate the size and morphology of Au nanoparticles. For the sample preparation of FE-SEM, an FTO glass was soaked in the as-synthesized Au colloid for 3 h. Optical properties were measured by an UV-Vis spectrophotometer (Lambda 35: Perkin-Elmer). For the extinction and diffused reflectance measurements of films, an integrated sphere was equipped to the spectrophotometer [25].

Photocurrent-voltage curves and electrochemical impedance spectra were obtained using a solar simulator (PEC-L11: Peccell) and potentiostat (CHI 608C: CH Instruments) under simulated solar illumination (AM 1.5 at 100 mW/cm^2). Incident photon-to-current conversion efficiency (*IPCE*) spectra were obtained by using an *IPCE* measurement system (K3100: Mcscience).

2.3. Results and Discussion

The extinction peak of the as-synthesized colloidal Au is observed at ~560 nm (Fig. 2-1), corresponding to the 100 nm-diameter Au nanoparticles [18,26]. The FE-SEM image again confirms the spherical Au nanoparticles with ~100 nm diameters (inset of Fig. 2-1).

Figure 2-2 shows the current density-voltage (*J*-*V*) characteristics and the incident photon-to-current conversion efficiency (*IPCE*) spectra. The power-conversion efficiency (η) of the DSSCs exhibits a maximum at the Au/TiO_2 mass ratio of ~0.05, and rapidly decreases at 0.07. The enhanced solar cell properties are attributed to the increased current density, while the open-circuit voltage (V_{oc}) and fill factor of the DSSCs are not notably changed by the addition of Au nanoparticles. In addition, the *IPCE*-enhancement ratio in the Au/TiO_2-DSSCs is more noticeable at longer wavelengths (inset of Fig. 2-2(b)).

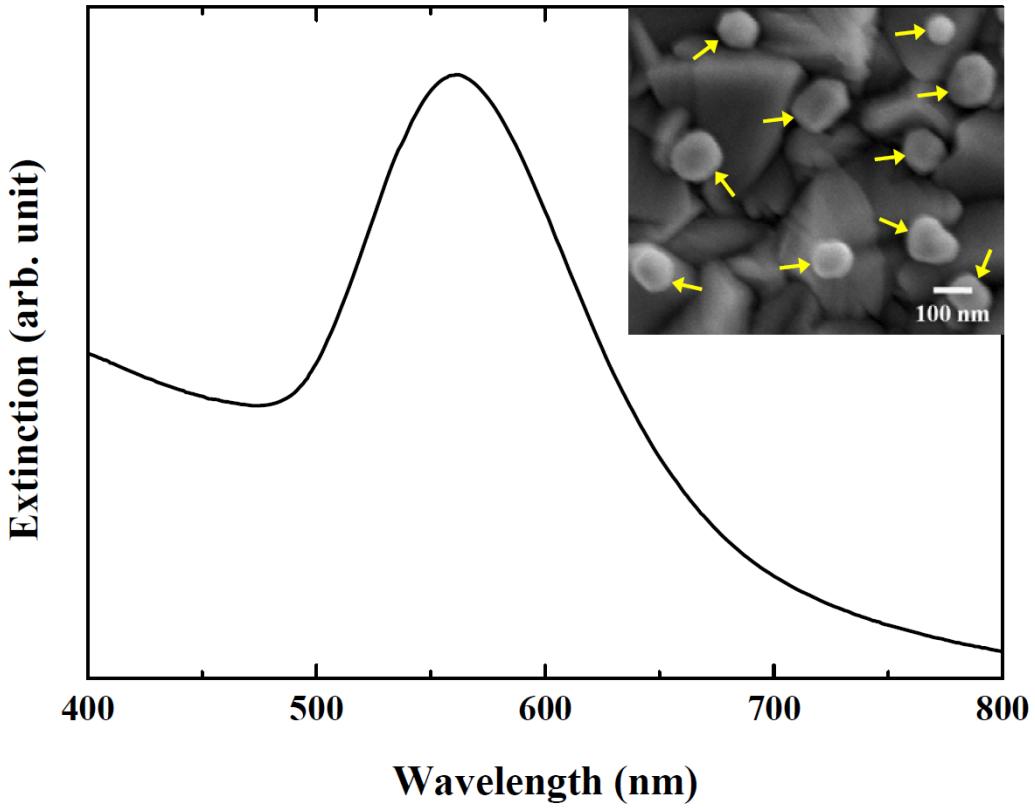

Fig. 2-1. (Color) UV-Vis extinction spectrum of the colloidal Au nanoparticles. The inset shows the FE-SEM image of Au nanoparticles on FTO grains.

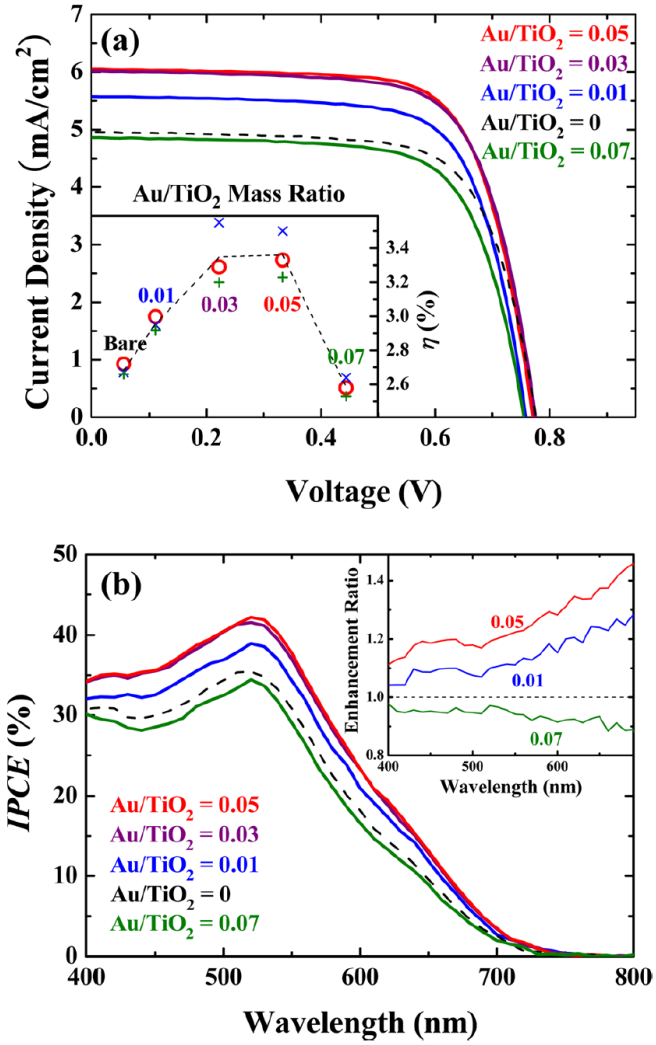

Fig. 2-2. (Color) (a) Photocurrent density-voltage (*J-V*) characteristics of DSSCs at various Au/TiO_2 mass ratios. The inset shows the power-conversion efficiency (η) of DSSCs with respect to the Au/TiO_2 mass ratio. (b) Incident photon-to-current conversion efficiency (*IPCE*) spectra of DSSCs at various Au/TiO_2 mass ratios. The *IPCE*-enhancement ratios are also shown compared with the bare DSSC ($Au/TiO_2 = 0$) in the inset.

To investigate the optical role of the Au nanoparticles, extinction and diffused reflectance of Au/TiO_2 films without dye were obtained. By measurements with an integrated sphere, scattered transmission and scattered reflection of films were detected, and as a result, absorption at the films was precisely calculated. Extinction is defined by the ratio of the transmitted-light intensity (I) to the incident-light intensity (I_0), representing the degree of both absorption and reflection:

$$\text{extinction} = -\log (I / I_0) = -\log T \quad (1)$$

$$A + R + T = 1 \quad (2)$$

where A, R, and T are absorptance, diffused reflectance, and transmittance, respectively. In this study, scattering and absorption by Au can be qualitatively separated by measuring diffused reflectance, because the Au nanoparticles in the optically quasi-isotropic matrix, consisting of the randomly distributed TiO_2 nanoparticles, scatter light also isotropically [2]. The backward-scattered light proceeds to the integrated sphere and contributes to the diffused reflectance [25]. In Fig. 2-3(a), the Au/TiO_2 film (mass ratio 0.05) exhibits higher extinction than the TiO_2 film, but shows a lower reflectance and consequentially higher absorptance at the wavelength of the surface-plasmon resonance of Au (Fig. 2-3(b)). These results indicate that the stronger extinction of Au/TiO_2 is attributed to absorption rather than scattering. Thus, the excessive addition of Au nanoparticles would be detrimental to absorption at the photoactive materials [27], and experimentally, photocurrent and power-conversion efficiency of DSSC drop when the Au/TiO_2 mass ratio was 0.07 (Fig. 2-2).

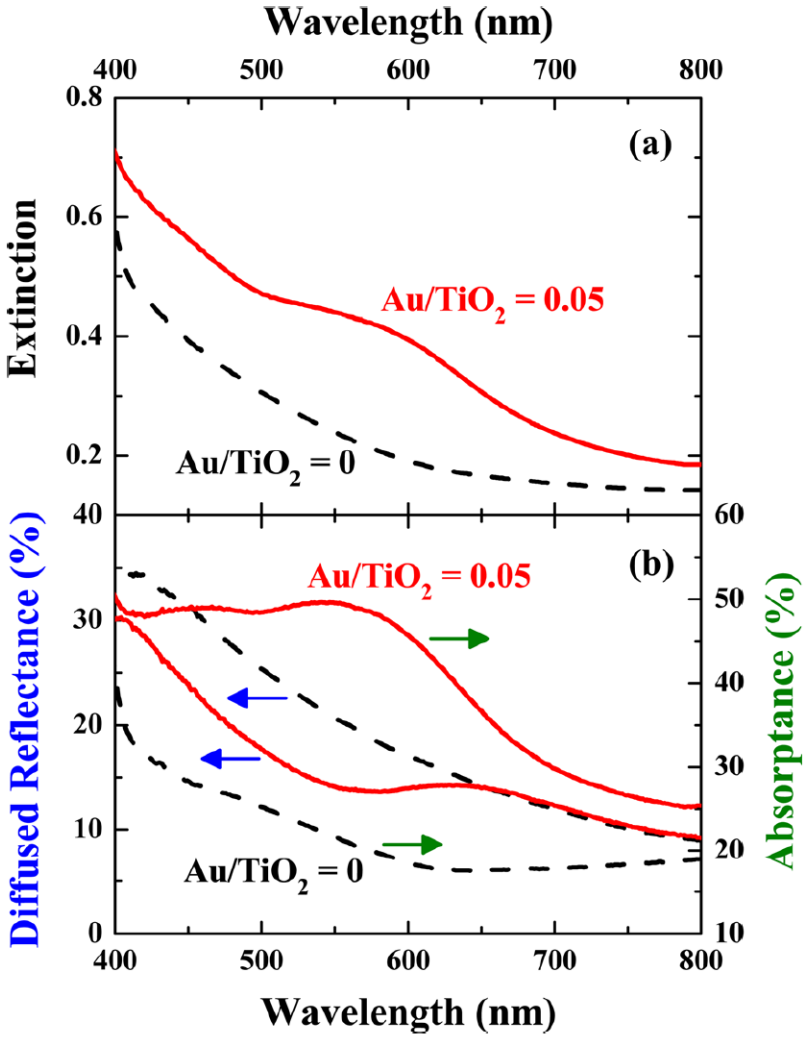

Fig. 2-3. (Color) (a) Extinction of Au/TiO_2 film (solid-red line) and TiO_2 film (dashed-black line) before dye adsorption. (b) Diffused reflectance (blue arrows) and absorptance (green arrows) of films before dye adsorption.

Surface-plasmon resonance of metal nanoparticles enhances the optical process: scattering and absorption. The relative strengths of these processes are expressed as cross sections, and the corresponding cross sections for scattering and absorption, C_{sca} and C_{abs}, can be calculated using the dielectric function of metal (ε_m) and medium material (ε_d):

$$C_{sca} = \left(\frac{1}{6\pi}\right)\left(\frac{2\pi}{\lambda}\right)^4 \cdot 9V^2 \left|\frac{\varepsilon_m - \varepsilon_d}{\varepsilon_m + 2\varepsilon_d}\right|^2 \text{and } C_{abs} = \frac{2\pi}{\lambda} \cdot 3V \cdot \text{Im}\left[\frac{\varepsilon_m - \varepsilon_d}{\varepsilon_m + 2\varepsilon_d}\right],$$

where λ and V are the wavelength of the incident light and the volume of the metal nanoparticle, respectively [2]. Scattering efficiency by plasmonic resonance is defined as $C_{sca} / (C_{sca} + C_{abs})$.

A 100 nm-diameter Au nanoparticle exhibits scattering efficiency of ~40% around the resonance frequency, and this value is much lower compared with a Ag nanoparticle of the same size showing over 80% in visible range (Fig. 2-4). Despite the relatively large size of Au nanoparticles, the higher imaginary part of dielectric function of Au gives rise to the dominant absorption-nature from surface-plasmon resonance, and thereby induces strong absorption of Au/TiO_2 film in this experiment.

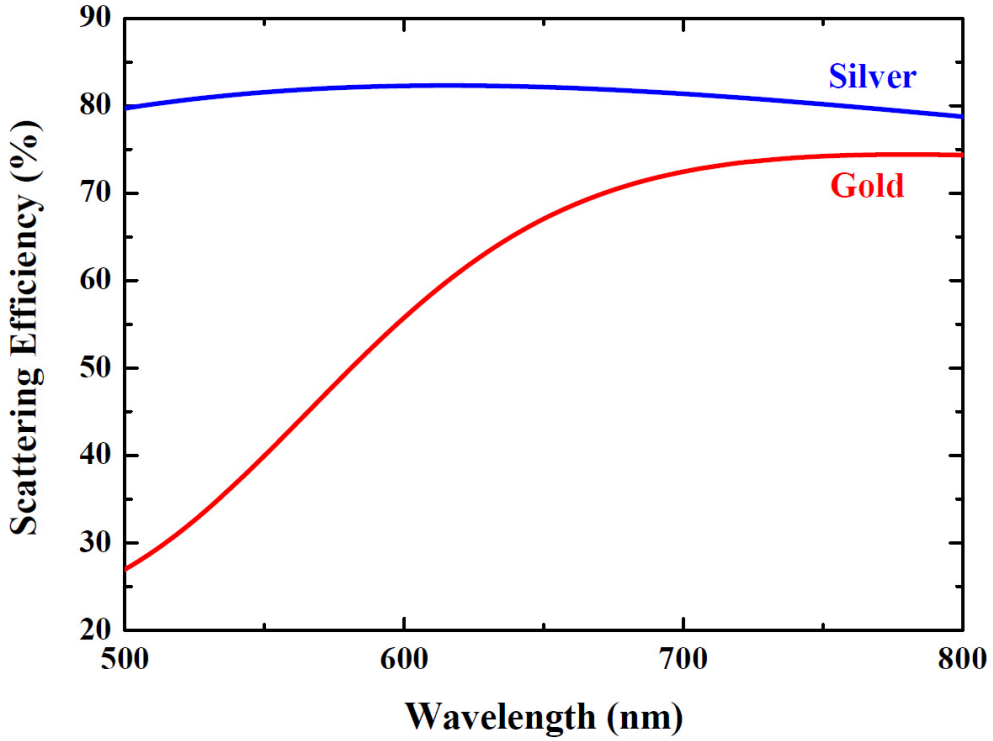

Fig. 2-4. (Color) Calculated scattering efficiency of Au and Ag nanoparticles, with a diameter of 100 nm. For the calculation of scattering efficiency, the dielectric function of Au and Ag were adopted from polynomial fitting to the measured data [28], and the dielectric function of medium (ε_d) was assumed as $2 + 0 \cdot i$.

The optical properties of the dye-adsorbed films were also measured. The Au/TiO_2 film exhibits stronger extinction (Fig. 2-5(a)) but similar reflectance spectra (Fig. 2-5(b)) compared with the bare TiO_2 film, over the whole wavelength region. The resultant absorptance data in Fig. 2-5(b) indicate that the dye-adsorbed Au/TiO_2 film absorbs much more photons than the dye-adsorbed bare TiO_2 film, particularly at the longer wavelengths. In addition, absorptance spectra are consistent with the *IPCE*-enhancement ratios, showing gradual rise as the wavelength increases (inset of Fig. 2-2(b)). Correlation between absorptance and *IPCE* indicates that the performance improvement of the Au/TiO_2-DSSCs is attributed to the enhancement of light absorption induced by the Au nanoparticles.

The Au/TiO_2 solar cells without dye were fabricated to examine direct photocarrier generation from Au nanoparticles [29]. However, there are no remarkable differences between Au/TiO_2 and bare TiO_2 electrodes (Fig. 2-6), and their photocurrent density and efficiency are low enough (~0.2 mA/cm^2 and ~0.05%, respectively). These results confirm that the direct photocarrier generation from Au is not the origin of the enhancement in the Au/TiO_2-DSSCs.

Electrochemical reactions taking place at the interfaces of DSSCs can be analyzed by electrical impedance spectroscopy [30]. In Bode plots, peak frequencies related to the electron lifetime in the TiO_2 films are similar between the two DSSCs (Fig. 2-7(b)), and this result indicates that the Au nanoparticles in DSSCs do not make critical changes in electron transport and recombination reactions.

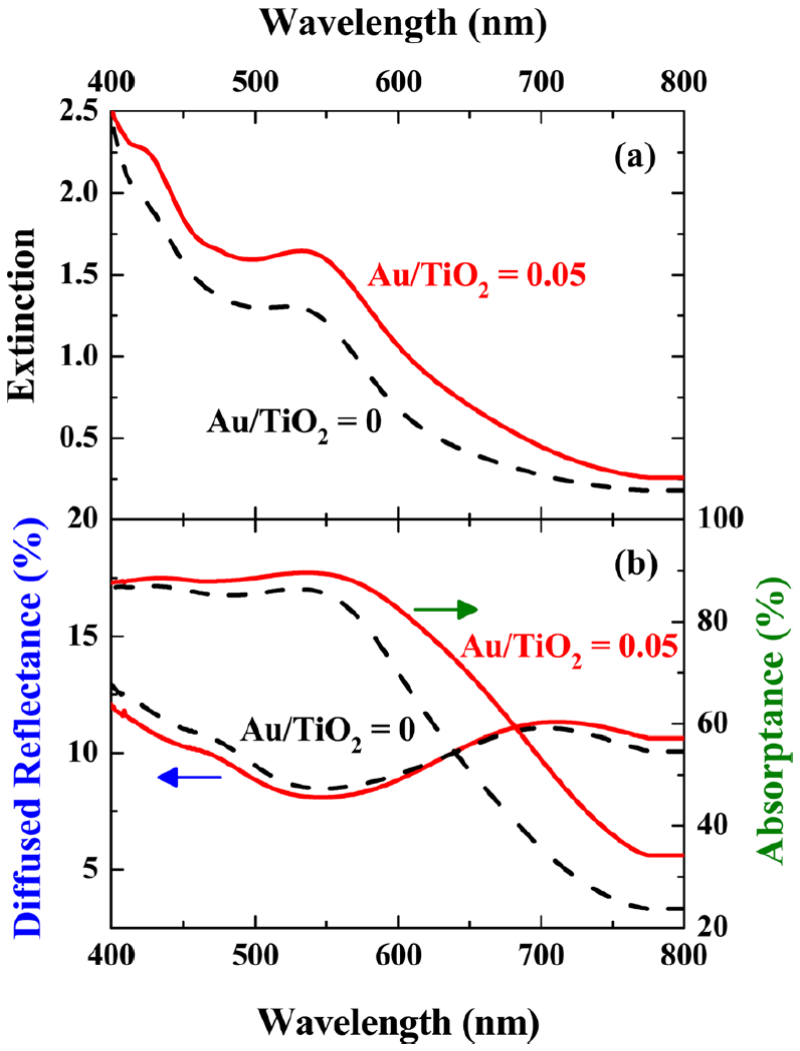

Fig. 2-5. (Color) (a) Extinction of Au/TiO_2 film (solid-red line) and TiO_2 film (dashed-black line) after dye adsorption. (b) Diffused reflectance (blue arrows) and absorptance (green arrows) of films after dye adsorption.

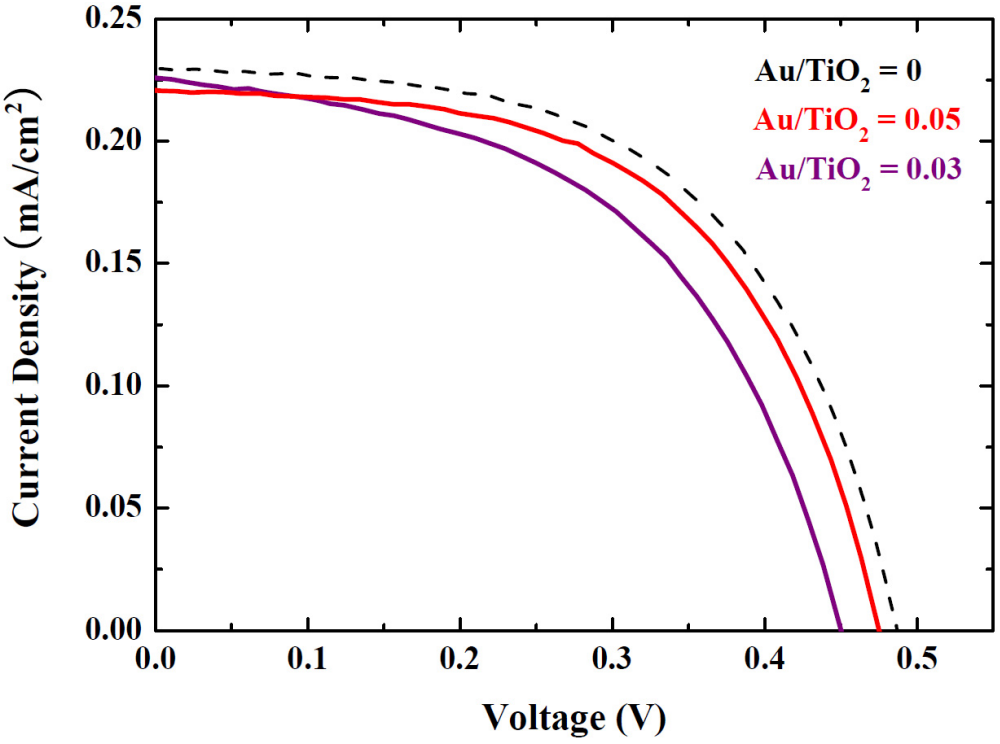

Fig. 2-6. (Color) Photocurrent density-voltage (*J-V*) characteristics of DSSCs without dye.

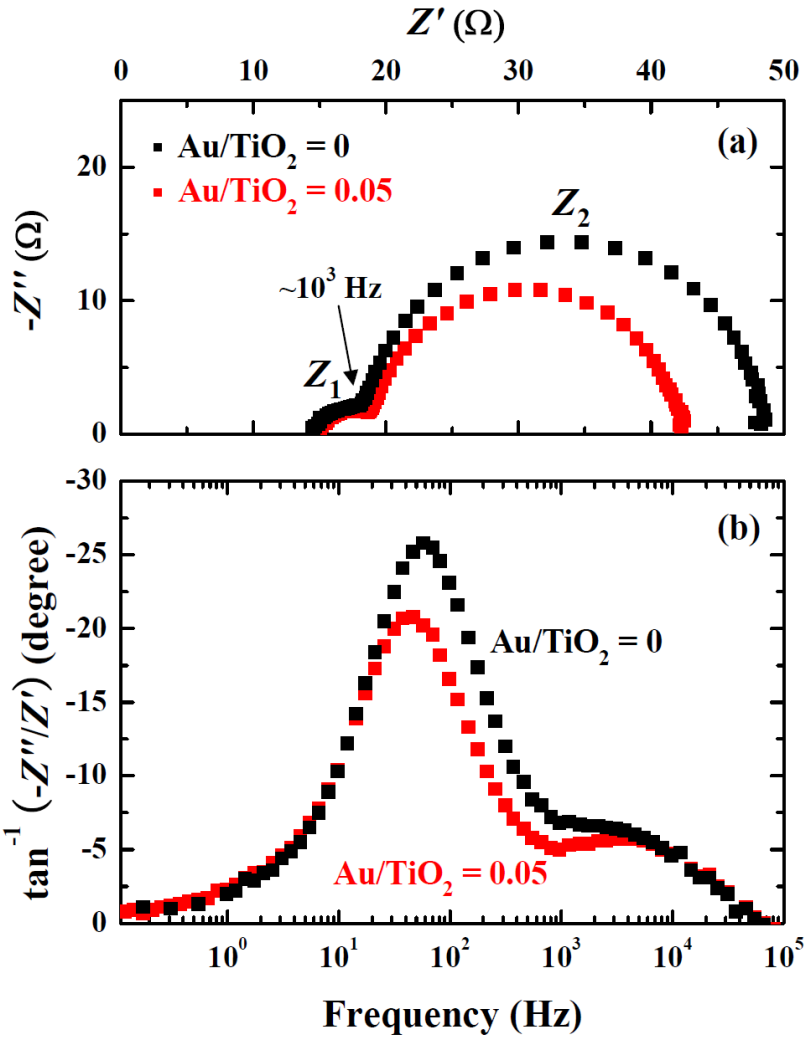

Fig. 2-7. (Color) Electrochemical impedance spectra measured at open-circuit voltage: (a) Nyquist plots and (b) Bode plots. In Nyquist plots, two semicircles in the frequency regions of 10^3 - 10^5 and 1 - 10^3 Hz correspond to impedances related to the Pt/electrolyte interface (Z_1) and TiO_2/dye/electrolyte interface (Z_2), respectively.

The field-enhancement effect in the vicinity of metal nanoparticles is a strong candidate for explaining the enhancement of light absorption and thereby improvement of the photovoltaic performances [3,31]. The electric field of incident light is strongly amplified by the oscillating surface charges in metal nanoparticles, and light absorption increases in proportion to the square of the electric-field amplitude [32,33]. In this research, Au nanoparticles in DSSC improved absorption of photoelectrode (Fig. 2-5(b)) and generation of photocurrent (Fig. 2-2), in spite of the demerit that Au nanoparticles themselves strongly absorb visible light (Fig. 2-3(b)). Although the field-enhancement effect is greatest at the surface-plasmon peak of metal, it is still over unity at other wavelengths [8,33], and this leads to the improvement of *IPCE* in the entire wavelength (inset of Fig. 2-2(b)). Previous researches of metal-induced DSSC have reported similar tendency that the photocurrent enhancement is observed along the whole wavelength region [13,16].

Metal nanoparticles also generate quenching processes [34], such as charge transfer and energy transfer to metals, which hamper the carrier generation at the active material. For higher enhancement by metal nanoparticles, quenching processes should be suppressed, or more specifically, the rate of electron-hole separation ($1/\tau_{separation}$) should be much faster than the rate of the quenching reaction by the metal ($1/\tau_{metal}$) [35]. Although τ_{metal} is dramatically changed by the distance from the metal, the wavelength of incident light, and the dielectric function of materials, values over 100 ps were obtained [36]. In the case of the DSSCs, it is widely accepted that the time constant for charge separation at the dye-TiO_2 interface ($\tau_{separation}$) is sub-picosecond [37]. Consequently, it is

expected that the quenching reaction would be negligible, since $\tau_{separation} << \tau_{metal}$, thus the field-enhancement effect dominantly influences the performance of DSSCs. A possible mechanism of the surface-plasmon resonance in the Au/TiO_2-DSSCs is schemed in Fig. 2-8.

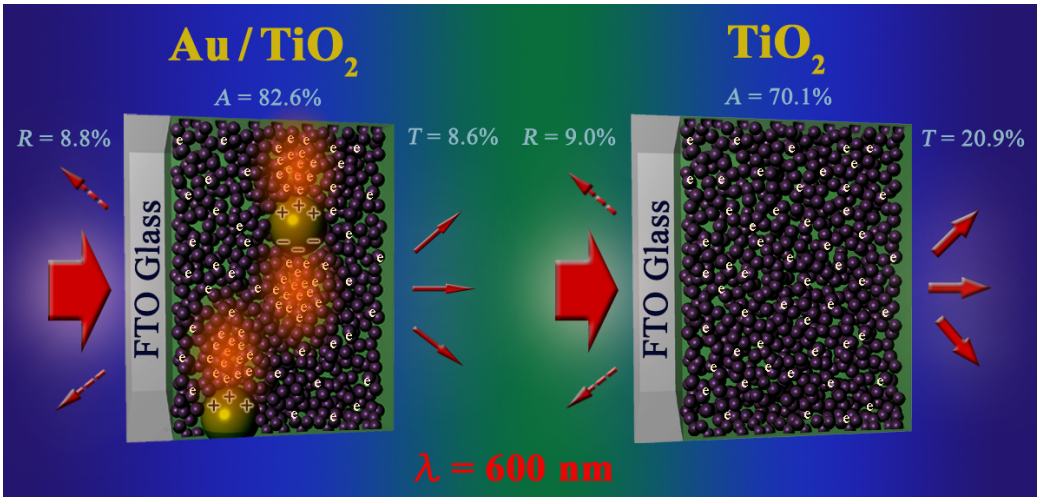

Fig. 2-8. (Color) Schematic figure representing the enhancement of Au/TiO_2-DSSC. Field enhancement near the Au nanoparticles is depicted as orange-color regions.

2.5. Conclusions

We incorporated 100 nm-diameter Au nanoparticles into the photoelectrode of DSSCs, and the power-conversion efficiency of DSSCs increased by ~20%. The 100 nm Au nanoparticles and Au/TiO_2 films exhibited unique light extinction caused by the localized surface-plasmon resonance, and this extinction in the DSSCs gave rise to effective light absorption by the field-enhancement effect rather than by prolonged optical-path lengths from scattering. By the simple analytic calculation, plasmonic effects of Au nanoparticles on DSSC can be understood, and the calculated results explain the experimental results with accuracy.

2.6. References

1. P. Mulvaney, “Surface Plasmon Spectroscopy of Nanosized Metal Particles,” *Langmuir* **12**, 788 (1996).
2. C. F. Bohren and D. R. Huffman, *Absorption and Scattering of Light by Small Particles*, Wiley, New York (1983).
3. P. Anger, P. Bharadwaj, and L. Novotny, “Enhancement and Quenching of Single-Molecule Fluorescence,” *Phys. Rev. Lett.* **96**, 113002 (2006).
4. D. L. Jeanmaire and R. P. Van Duyne, “Surface Raman Spectroelectrochemistry: Part I. Heterocyclic, Aromatic, and Aliphatic Amines Adsorbed on the Anodized Silver Electrode,” *J. Electroanal. Chem.* **84**, 1 (1977).
5. E. C. Nelson and P. V. Braun, “Enhancing Colloids Through the Surface,” *Science* **318**, 924 (2007).
6. Y. C. Cao, R. Jin, and C. A. Mirkin, “Nanoparticles with Raman Spectroscopic Fingerprints for DNA and RNA Detection,” *Science* **297**, 1536 (2002).
7. D.-R. Jung, J. Kim, S. Nam, C. Nahm, H. Choi, J. I. Kim, J. Lee, C. Kim, and B. Park, “Photoluminescence Enhancement in CdS Nanoparticles by Surface-Plasmon Resonance,” *Appl. Phys. Lett.* **99**, 041906 (2011).
8. H. A. Atwater and A. Polman, “Plasmonics for Improved Photovoltaic Devices,” *Nat. Mater.* **9**, 205 (2010).
9. D. Derkacs, S. H. Lim, P. Matheu, W. Mar, and E. T. Yu, “Improved Performance of Amorphous Silicon Solar Cells via Scattering from Surface Plasmon Polaritons in

nearby Metallic Nanoparticles," *Appl. Phys. Lett.* **89**, 093103 (2006).

10. K. Nakayama, K. Tanabe, and H. A. Atwater, "Plasmonic Nanoparticle Enhanced Light Absorption in GaAs Solar Cells," *Appl. Phys. Lett.* **93**, 121904 (2008).
11. J.-L. Wu, F.-C. Chen, Y.-S. Hsiao, F.-C. Chien, P. Chen, C.-H. Kuo, M. H. Huang, and C.-S. Hsu, "Surface Plasmonic Effects of Metallic Nanoparticles on the Performance of Polymer Bulk Heterojunction Solar Cells," *ACS Nano* **5**, 959 (2011).
12. B. P. Rand, P. Peumans, and S. R. Forrest, "Long-Range Absorption Enhancement in Organic Tandem Thin-Film Solar Cells Containing Silver Nanoclusters," *J. Appl. Phys.* **96**, 7519 (2004).
13. S. D. Standridge, G. C. Schatz, and J. T. Hupp, "Distance Dependence of Plasmon-Enhanced Photocurrent in Dye-Sensitized Solar Cells," *J. Am. Chem. Soc.* **131**, 8407 (2009).
14. S. D. Standridge, G. C. Schatz, and J. T. Hupp, "Toward Plasmonic Solar Cells: Protection of Silver Nanoparticles via Atomic Layer Deposition of TiO_2," *Langmuir* **25**, 2596 (2009).
15. M. D. Brown, T. Suteewong, R. S. S. Kumar, V. D'Innocenzo, A. Petrozza, M. Lee, U. Wiesner, and H. J. Snaith, "Plasmonic Dye-Sensitized Solar Cells Using Core-Shell Metal-Insulator Nanoparticles," *Nano Lett.* **11**, 438 (2011).
16. M. Ihara, M. Kanno, and S. Inoue, "Photoabsorption-Enhanced Dye-Sensitized Solar Cell by Using Localized Surface Plasmon of Silver Nanoparticles Modified with Polymer," *Physica E* **42**, 2867 (2010).
17. D. D. Evanoff and G. Chumanov, "Size-Controlled Synthesis of Nanoparticles. 2.

Measurement of Extinction, Scattering, and Absorption Cross Sections," *J. Phys. Chem. B* **108**, 13957 (2004).

18. J. Kimling, M. Maier, B. Okenve, V. Kotaidis, H. Ballot, and A. Plech, "Turkevich Method for Gold Nanoparticle Synthesis Revisited," *J. Phys. Chem. B* **110**, 15700 (2006).
19. Md. K. Nazeeruddin, R. Humphry-Baker, and M. Grätzel, "Investigation of Sensitizer Adsorption and the Influence of Protons on Current and Voltage of a Dye-Sensitized Nanocrystalline TiO_2 Solar Cell," *J. Phys. Chem. B* **107**, 8981 (2003).
20. S. Ito, P. Chen, P. Comte, M. K. Nazeeruddin, P. Liska, P. Péchy, and M. Grätzel, "Fabrication of Screen-Printing Pastes from TiO_2 Powders for Dye-Sensitized Solar Cells," *Prog. Photovoltaics* **15**, 603 (2007).
21. G. P. Smestad and M. Grätzel, "Demonstrating Electron Transfer and Nanotechnology: a Natural Dye-Sensitized Nanocrystalline Energy Converter," *J. Chem. Educ.* **75**, 752 (1998).
22. N.-G. Park, J. van de Lagemaat, and A. J. Frank, "Comparison of Dye-Sensitized Rutile- and Anatase-Based TiO_2 Solar Cells," *J. Phys. Chem. B* **104**, 8989 (2000).
23. R. L. Willis, C. Olson, B. O'Regan, T. Lutz, J. Nelson, and J. R. Durrant, "Electron Dynamics in Nanocrystalline ZnO and TiO_2 Films Probed by Potential Step Chronoamperometry and Transient Absorption Spectroscopy," *J. Phys. Chem. B* **106**, 7605 (2002).
24. H. S. Jung, J.-K. Lee, M. Nastasi, S.-W. Lee, J.-Y. Kim, J.-S. Park, K. S. Hong, and H. Shin, "Preparation of Nanoporous MgO-Coated TiO_2 Nanoparticles and Their

Application to the Electrode of Dye-Sensitized Solar Cells," *Langmuir* **21**, 10332 (2005).

25. H.-J. Koo, J. Park, B. Yoo, K. Yoo, K. Kim, and N.-G. Park, "Size-Dependent Scattering Efficiency in Dye-Sensitized Solar Cell," *Inorg. Chim. Acta* **361**, 677 (2008).
26. L. M. Liz-Marzan, "Tailoring Surface Plasmons through the Morphology and Assembly of Metal Nanoparticles," *Langmuir* **22**, 32 (2006).
27. V. P. Zhdanov, "On the Use of Metal Nanoparticles for Enhamcenet of Light Absorption in Dye-Sensitized Soalr Cells," *Physica E* **43**, 494 (2010).
28. E. D. Palik, *Handbook of Optical Constants of Solids*, Academic, San Diego (1985**)**.
29. Z. H. Chen, Y. B. Tang, C. P. Liu, Y. H. Leung, G. D. Yuan, L. M. Chen, Y. Q. Wang, I. Bello, J. A. Zaipen, W. J. Zhang, C. S. Lee, and S. T. Lee, "Vertically Aligned ZnO Nanorod Arrays Sensitized with Gold Nanoparticles for Schottky Barrier Photovoltaic Cells," *J. Phys. Chem. C* **113**, 13433 (2009).
30. L. Han, N. Koide, Y. Chiba, and T. Mitate, "Modeling of an Equivalent Circuit for Dye-Sensitized Solar Cells," *Appl. Phys. Lett.* **84**, 2433 (2004).
31. C. Hägglund, M. Zäch, and B. Kasemo, "Enhanced Charge Carrier Generation in Dye Sensitized Solar Cells," *Appl. Phys. Lett.* **92**, 013113 (2008).
32. J.-Y. Lee and P. Peumans, "The Origin of Enhanced Optical Absorption in Solar Cells with Metal Nanoparticles Embedded in the Active Layer," *Opt. Express* **18**, 10078 (2010).
33. K. Tanabe, "Field Enhancement around Metal Nanoparticles and Nanoshells: a

Systematic Investigation," *J. Phys. Chem. C* **112**, 15721 (2008).

34. E. Dulkeith, M. Ringler, T. A. Klar, J. Feldmann, A. Muñoz Javier, and W. J. Parak, "Gold Nanoparticles Quench Fluorescence by Phase Induced Radiative Rate Suppression," *Nano Lett.* **5**, 585 (2005).
35. A. O. Govorov and I. Carmeli, "Hybrid Structures Composed of Photosynthetic System and Metal Nanoparticles: Plasmon Enhancement Effect," *Nano Lett.* **7**, 620 (2007).
36. A. O. Govorov, G. W. Bryant, W. Zhang, T. Skeini, J. Lee, N. A. Kotov, J. M. Slocik, and R. R. Naik, "Exciton-Plasmon Interaction and Hybrid Excitons in Semiconductor-Metal Nanoparticle Assemblies," *Nano Lett.* **6**, 984 (2006).
37. A. Hagfeldt, G. Boschloo, L. Sun, L. Kloo, and H. Pettersson, "Dye-Sensitized Solar Cells," *Chem. Rev.* **110**, 6595 (2010).
38. K. A. Willets and R. P. Van Duyne, "Localized Surface Plasmon Resonance Spectroscopy and Sensing," *Annu. Rev. Phys. Chem.* **58**, 267 (2007).
39. E. D. Palik, *Handbook of Optical Constants of Solids* (Academic, San Diego, CA, 1985).
40. A. Peic, D. Staff, T. Risbridger, B. Menges, L. M. Peter, A. B. Walker, and P. J. Cameron, "Real-Time Optical Waveguide Measurements of Dye Adsorption into Nanocrystalline TiO_2 Films with Relevance to Dye-Sensitized Solar Cells," *J. Phys. Chem. C* **115**, 613 (2011).
41. C. Nahm, D.-R. Jung, J. Kim, S. Nam, H. Choi, S. Hong, T. Hwang, T. Moon, and B. Park, "Photoluminescence Enhancement by Surface-Plasmon Resonance:

Recombination-Rate Theory and Experiments," *Appl. Phys. Express* **6**, 052001 (2013).

Chapter 3.

A Simple Template-Free 'Sputtering Deposition and Selective Etching' Process for Nanoporous Thin Films and Its Application to Dye-Sensitized Solar Cells

3.1. Introduction

Nanostructured electrodes have been applied to the various devices such as solar cells [1-5], lithium-ion batteries [6,7], polymer-electrolyte-membrane fuel cells [8,9], etc. Particularly, introduction of nanostructured photoelectrodes dramatically enhanced performances of dye-sensitized solar cells (DSSCs). The amount of dye adsorbed on the device increased due to the large surface area of nanoparticulate-TiO_2 photoelectrodes, and accordingly, both photocurrent and power-conversion efficiency of the DSSC were notably enhanced [10]. Recently reported high-performance DSSCs, showing power-conversion efficiencies over 12%, also used this nanoparticulate-TiO_2 film as the

---

The work presented in Chapter 3 is submitted to *Nanotechnology* entitled,
"A Simple Template-Free 'Sputtering Deposition and Selective Etching' Process for Nanoporous Thin Films and Its Application to Dye-Sensitized Solar Cells."
Changwoo Nahm, Hongsik Choi, Jongmin Kim, Sujin Byun, Suji Kang, Taehyun Hwang, Helen Hejin Park, Jaejung Ko,* and Byungwoo Park*

photoelectrode [11].

Hydrothermally-synthesized TiO_2 nanoparticles are conventionally used for the photoelectrode materials of DSSCs. Synthesized colloidal nanoparticles are converted to viscous paste, and then the paste is deposited on a substrate either by screen printing [12] or doctor-blade method [13]. This conventional process guarantees high efficiencies of devices, but the process itself is time-consuming and repetitive. Other approaches to synthesize the nanostructured-TiO_2 photoelectrode have been suggested, such as growth of nanorods or nanotubes [14-16], template-assisted method [17-19], and anodization of Ti foil [20], but they have common problems of complex and difficult experimental procedures and poor reproducibilities.

Another candidate for the deposition of TiO_2-photoelectrodes is by sputtering. With the merits of large-area deposition, high uniformity, and good reproducibility, sputtering deposition has been widely utilized in industrial field to obtain various coating layers and high-quality functional films [21]. However, TiO_2 films grown by sputtering have compact structures with low surface area, thus showing inferior properties as DSSC-photoelectrodes compared to the nanoparticulate-TiO_2 films [22,23]. To overcome this problem, selective-etching can be directly applied. In alloy systems, electrochemically more active species are selectively etched by chemical reaction or applying voltage, and consequently nanoporous structures composed of novel metals are synthesized, as shown in Fig. 3-1 [24,25].

In this research, we introduce a facile and effective method to fabricate nanoporous-TiO_2 thin films, with sputtering and subsequent selective etching. First,

silver/TiO_2 nanocomposite thin films were deposited by co-sputtering (left scheme in Fig. 3-2). Since the surface tension of metal is larger than that of metal-oxide [26-29], silver atoms agglomerate and form nanoclusters in the film. Then, silver nanoclusters in the nanocomposite were selectively etched in nitric acid by [24,30]:

$$Ag + 2HNO_3 \rightarrow Ag^+ + NO_3^- + H_2O + NO_2.$$

The remaining TiO_2 thin film with nanoporous structure is described in the right scheme of Fig. 3-2.

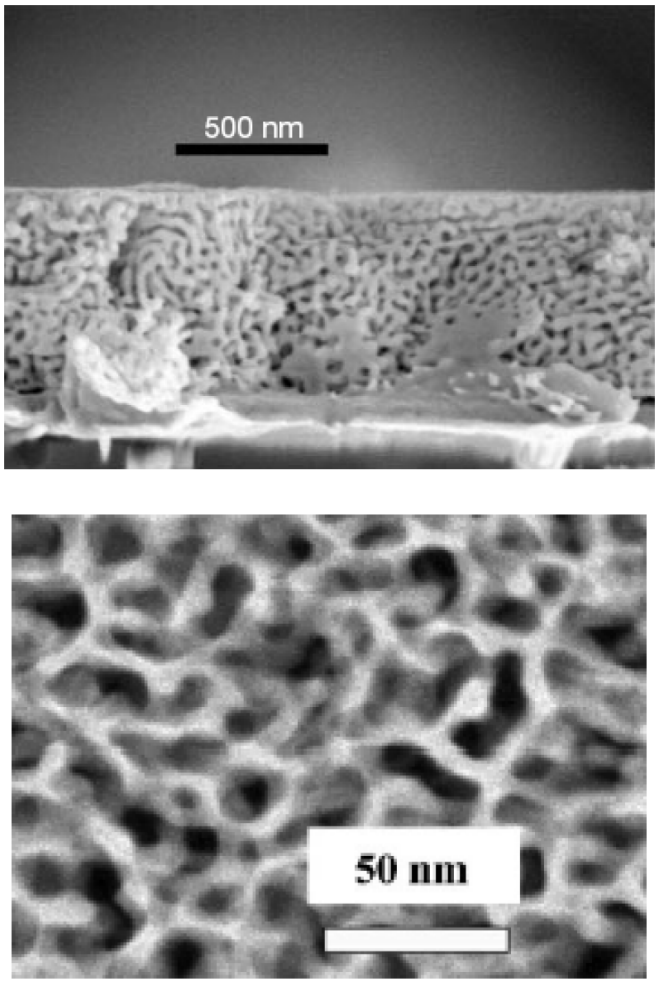

Fig. 3-1. Metallic nanoporous structure fabricated from selective etching. (upper) Nanoporous Au thin film from Ag-Au alloys. From Ref. [24]. (lower) Nanoporous Pt thin film from Pt_xSi_{1-x} alloys. From Ref. [25].

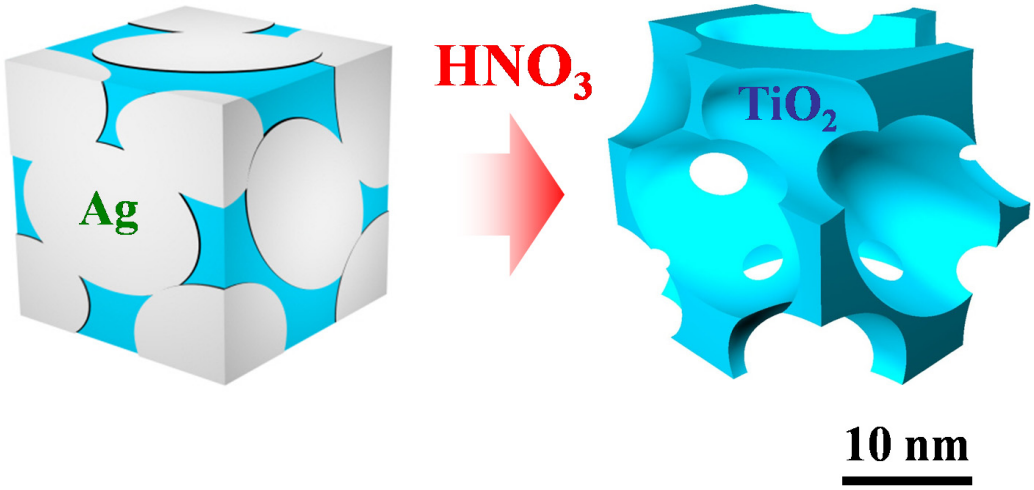

Fig. 3-2. (Color) Schematic figure representing a method for fabricating nanoporous-TiO_2 thin films.

3.2. Experimental Section

Ag/TiO_2 thin films were deposited on FTO glass (for DSSC fabrication) or Si (100) wafer (for x-ray analysis) by rf magnetron sputtering using Ag and TiO_2 targets of 2-inch in diameter. Sputtering was performed in an Ar atmosphere with working pressure of 5 mTorr at room temperature. To find optimum conditions, sputtering power of Ag was varied while that of TiO_2 was fixed at 100 W. For the comparison, bare-TiO_2 thin films were also prepared with TiO_2 sputtering power of 100 W, without Ag co-sputtering.

To selectively etch Ag from Ag/TiO_2 films, as-deposited Ag/TiO_2 thin films were immersed in diluted nitric acid (70 wt. % HNO_3/deionized H_2O, with the volume ratio of 1:2) for 1 min. Concentration of HNO_3 solution (volume ratio of HNO_3/H_2O from 1:1 to 1:3) and etching time (from 1 to 10 min) did not critically influence the results in this research. HNO_3-treated films were washed in deionized H_2O and ethanol, and annealed in a box furnace at 500°C for 2 h to crystallize remaining TiO_2. Annealed films were additionally treated with aqueous solution of titanium tetrachloride ($TiCl_4$: Aldrich, St. Louis, USA) to improve the solar-cell performance. Experimental details for the $TiCl_4$ treatment follow the previous research, and dipping time is optimized in terms of power-conversion efficiency of DSSC. Pure $TiCl_4$ was added to pre-cooled (~0°C) deionized H_2O to make 40 mM $TiCl_4$ aqueous solution, and annealed films were dipped in this solution for 1 h at 70°C. Then, $TiCl_4$-treated films were annealed once again at 500°C for 2 h.

To fabricate DSSCs, annealed films were immersed in 0.3 mM anhydrous ethanol

solution of N719 dye ($RuL_2(NCS)_2$:2TBA, L = 2,2′-bipyridyl-4,4′-dicarboxylic acid, TBA = tetrabutylammonium: Solaronix) for 12 h at room temperature. The dye-adsorbed electrode and Pt thin film for the counter electrode were sealed with thermoplastic foil (Dupont), and an iodide-based redox electrolyte (AN-50: Solaronix) was injected into the gap between the two electrodes. Active area of DSSCs was fixed at 0.36 cm^2 by masking FTO surface during the sputtering deposition.

Phase of thin films was analyzed by x-ray diffraction (XRD, M18XHF-SRA: Mac Science, Japan). Density of thin films was examined by x-ray reflectivity (XRR, X'pert Pro: PANalytical, Netherland) and a simulation program (X'pert Reflectivity: PANalytical, Netherland). Field-emission scanning electron microscopy (FE-SEM, SU70: Hitachi, Japan) was used to investigate the nanostructure of thin films. In order to measure the amount of adsorbed dye on TiO_2 film, dyes were desorbed in a mixture of 0.1 M NaOH aqueous solution/ethanol with the volume ratio of 1:1, and absorption spectra of the resultant dye solutions were measured by an UV-visible spectrophotometer (Lambda 35: Perkin-Elmer, MA, USA). Photocurrent-voltage curves, electrochemical impedance spectra, and open-circuit voltage decay of DSSCs were obtained using a solar simulator (K3000: McScience, Korea) and potentiostat (CHI 608C: CH Instruments, TX, USA) under simulated solar illumination (AM 1.5 at 100 mW cm^{-2}). The electrochemical impedance spectra were recorded over a frequency range of 0.1 to 10^5 Hz, and applied bias voltage and AC amplitude were open-circuit voltage (V_{oc}) of the DSSC and 10 mV, respectively. Incident photon-to-current conversion efficiency (*IPCE*) spectra were obtained by using an *IPCE* measurement

system (K3100: McScience, Korea) at a chopping speed of 5 Hz.

3.3. Results and Discussion

X-ray diffraction (XRD) of the as-deposited Ag/TiO_2 nanocomposite thin film indicates peaks from the crystalline Ag (Fig. 3-3(a)). Grain size of Ag in the Ag/TiO_2 nanocomposite film is calculated as ~4 nm by the Scherrer equation [31,32], and this value is roughly verified by the transmission-electron-microscopic (TEM) image (Fig. 3-4). Several nanocomposites with different Ag-sputtering power were also analyzed, and the grain size of Ag gets bigger as the Ag-sputtering power is increased (Fig. 3-5). Absence of TiO_2 peaks in Fig. 3-3(a) and Fig. 3-5 is due to the amorphous nature in the as-deposited film. The Ag/TiO_2 thin-film nanocomposite (Fig. 3-3(a)) was immersed in HNO_3 to selectively etch Ag, and subsequent annealing at 500°C crystallized remaining TiO_2 (Fig. 3-3(b)). Transparency of the post-etched film in visible range, confirmed by UV-visible spectroscopy, also demonstrates the complete removal of Ag from the Ag/TiO_2 nanocomposite film (data not shown).

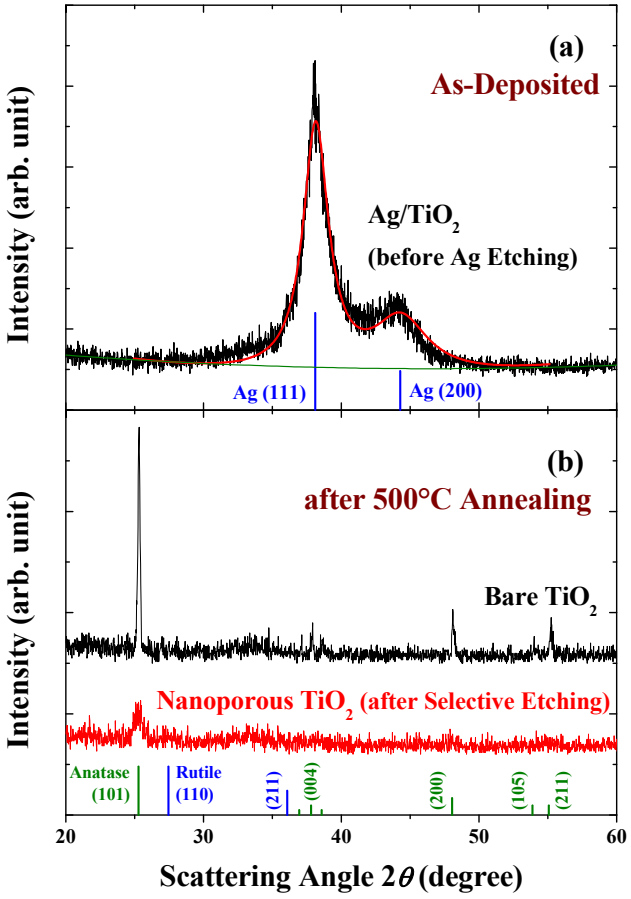

Fig. 3-3. (Color) (a) X-ray diffraction (XRD) pattern of the as-deposited Ag/TiO_2 film. Measured (black) and fitted (red) curves are superimposed. (b) XRD pattern of the nanoporous-TiO_2 film (red) prepared by dissolution of Ag from the Ag/TiO_2 film and subsequent annealing. For comparison, diffraction pattern of a bare-TiO_2 film (black) is also shown.

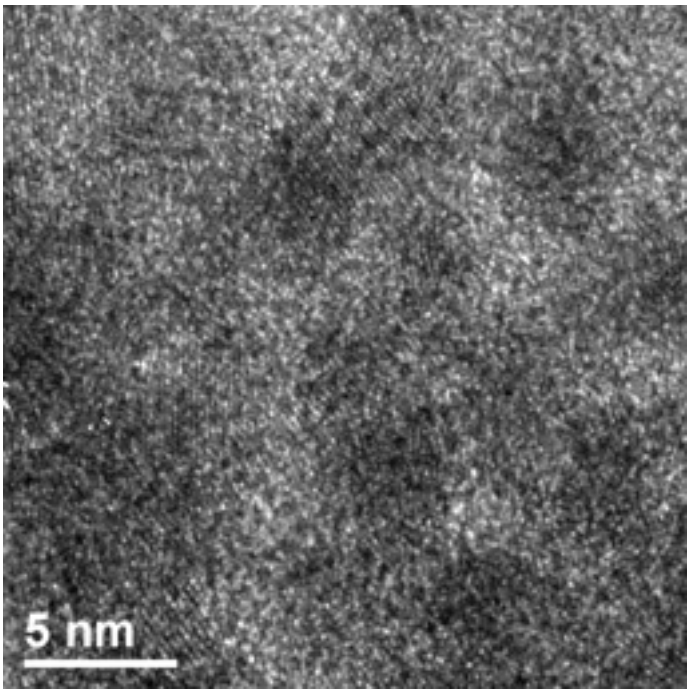

Fig. 3-4. TEM image of Ag/TiO_2 nanocomposite film.

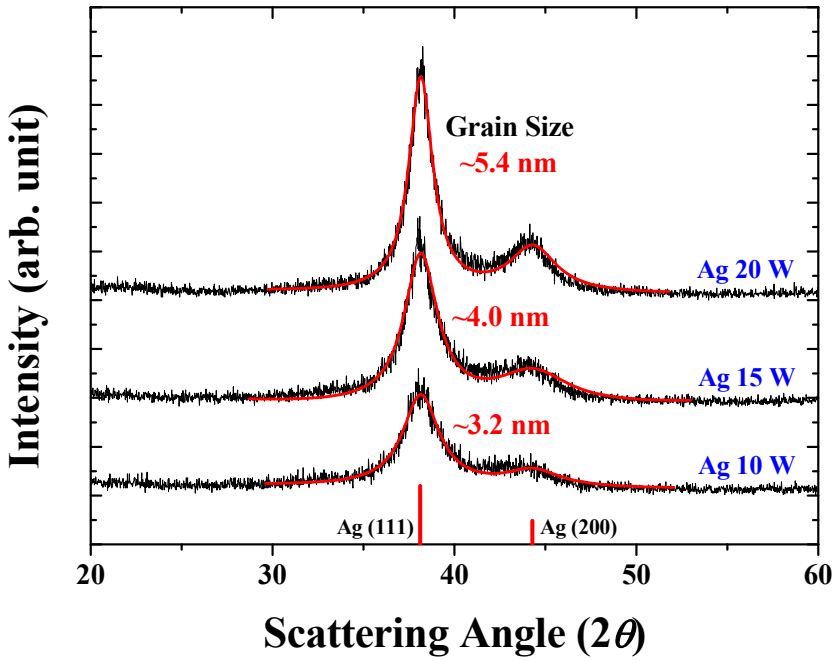

Fig. 3-5. (Color) XRD patterns of Ag/TiO_2 nanocomposite films with different Ag sputtering power.

Both electron microscopic images and x-ray reflectivity (XRR) spectra confirm the formation of nanoporous-TiO_2 film. Figure 3-6(a) clearly shows rough surface and porous morphology compared to Fig. 3-6(b) which exhibits planar surface and compact structure of the bare-TiO_2 film. With the same deposition time, the nanoporous-TiO_2 film is about twice thicker than the bare-TiO_2 film (Figs. 3-6(a) and 3-6(b)), and the selective etching of Ag did not change the thickness of film. Furthermore, XRR simulation reveals that density of the nanoporous-TiO_2 film is about 1.43 g cm^{-3} (Fig. 3-6(c)). This value corresponds to the film porosity of ~63%, with the assumption that the nanoporous film consists of pure TiO_2 anatase phase ($\rho_{anatase}$ = 3.89 g cm^{-3}). For the best performance of DSSCs, photoelectrodes should have proper porosity to support sufficient space for dye adsorption on TiO_2 surface and to provide pathways for iodide/triiodide ions in the electrolyte. Porosity of the conventional nanoparticulate-TiO_2 photoelectrode with the power-conversion efficiency of ~10% is approximately 65% [33], which is comparable with our nanoporous-TiO_2 thin film.

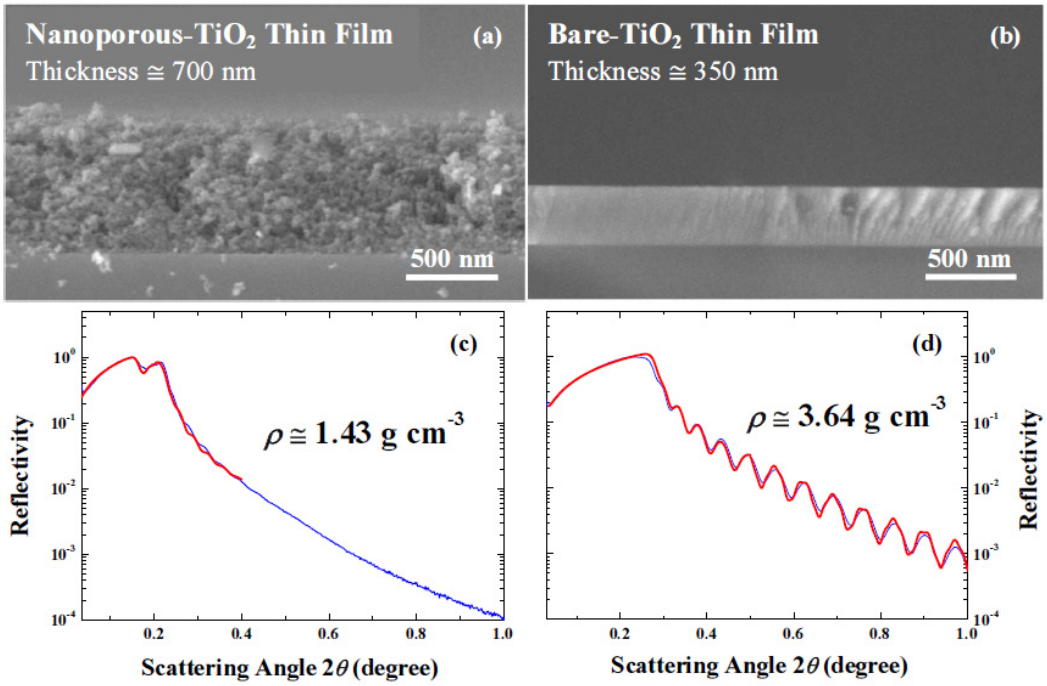

Fig. 3-6. (Color) Cross-sectional FE-SEM images of (a) the nanoporous-TiO_2 film and (b) the bare-TiO_2 film. X-ray reflection spectra of (c) the nanoporous-TiO_2 film and (d) the bare-TiO_2 film. Simulated spectra (red) are shown with the measured spectra (blue) in both (c) and (d). Deposition time was the same for both films.

Due to the nanoporous structure and concomitant large surface area, the nanoporous-TiO_2 film adsorbs much more dyes than the bare-TiO_2 film, as shown in Fig. 3-7. The amount of dye adsorbed on the nanoporous-TiO_2 film (0.7 μm thick, Fig. 3-6(a)), calculated from UV-visible absorption spectra in Fig. 4, is 2.26×10^{-8} mol cm^{-2}, and the corresponding surface area of the nanoporous film is 231.4 m^2 g^{-1} (Table 3-1) assuming that a single dye molecule adsorbs on TiO_2 within 1.7 nm^2 [1]. Since the conventional nanoparticulate-TiO_2 photoelectrode has a surface area of ~80 m^2 g^{-1} [33], the nanoporous-TiO_2 film is expected to contain much more dye and thereby exhibits improved solar-cell properties. In addition, average pore size in the nanoporous-TiO_2 film is estimated to be 7.7 nm (Table 3-1), with the cylindrical pore-shape assumption which is generally used to determine the nanoporosity in DSSCs. Although the calculated pore size is smaller than that of the typical nanoparticulate-TiO_2 film, it is supposed that this value is sufficient for iodide/triiodide ions in the electrolyte to operate DSSC normally [34].

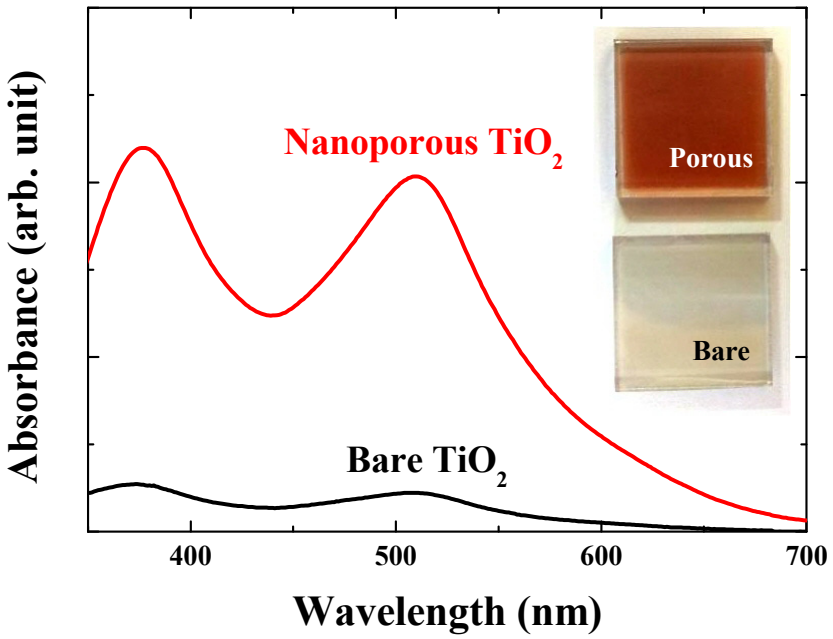

Fig. 3-7. (Color) Absorption spectra of desorbed dye solutions from the nanoporous-TiO_2 film (red) and the bare-TiO_2 film (black). Photo of dye-adsorbed TiO_2 films is shown in the inset.

Table 3-1. Porosity, surface area, and average pore size of the nanoporous-TiO_2 film. The values of the conventional nanoparticulate-TiO_2 film are also listed for comparison.

	Porosity	**Surface Area (m^2 g^{-1})**	**Average Pore Size (nm)**
Nanoporous TiO_2	**63.2%[a)]**	**231.4[b)]**	**7.7[c)]**
Conventional Nanoparticle TiO_2[d)]	**65.3%**	**86.0**	**20.2**

[a)] Calculated, with the assumption that the film consists of pure anatase phase ($\rho_{anatase}$ = 3.89 g cm^{-3}).

[b)] Calculated, with the assumption that a single dye molecule adsorbs on the TiO_2 surface with an area of 1.7 nm^2.

[c)] Calculated, with the cylindrical pore-shape assumption.

[d)] Values are referred from Ref. 33.

The nanoporous-TiO_2 thin-film DSSC exhibits much enhanced solar-cell properties than the bare-TiO_2 thin-film DSSC (dashed lines in Fig. 3-8 and Table 3-2). The higher power-conversion efficiency (η) of nanoporous-TiO_2 DSSC is mainly attributed to the increased current density, and this is consistent with the dye-loading data (Fig. 3-7). However, the DSSC with thicker nanoporous-TiO_2 film (1.8 μm) does not reach the expected current density and η (red solid line in Fig. 3-8), in spite of the increased dye loading proportional to the TiO_2 thickness (not shown).

Electron diffusion length $(D_e\tau)^{1/2}$ in DSSCs influences collection of photoelectrons. Electron diffusivity (D_e) of 1.8-μm-thick nanoporous-TiO_2 DSSC, obtained from the Nyquist plot at V_{oc} (Fig. 3-9) [35], is two orders of magnitude smaller than that of the conventional nanoparticulate-TiO_2 DSSC ($\sim 3 \times 10^{-5}$ cm^2 s^{-1}) [35,36], and the corresponding $(D_e\tau)^{1/2}$ is 1.24 μm ($\tau = 35$ ms from $\tau = (2\pi f)^{-1}$, where f stands for the frequency at the arc peak in the Nyquist plot [37]). This calculation indicates that the 1.8-μm-thick nanoporous-TiO_2 DSSC has a problem with the charge collection since photoelectrode is thicker than its $(D_e\tau)^{1/2}$. Charge-collection efficiency (η_{cc}) in DSSCs can be calculated by:

$$\eta_{cc} = (1 + \tau_{tr}/\tau)^{-1},$$

where τ_{tr} is the electron-transport time in the photoelectrode ($\tau_{tr} = d^2/2.5D_e$ with d for the photoelectrode thickness [1,38]). The value of η_{cc} in the 1.8-μm-thick nanoporous-TiO_2 DSSC is 54%, concerning that half of photogenerated electrons recombine before reaching the FTO electrode.

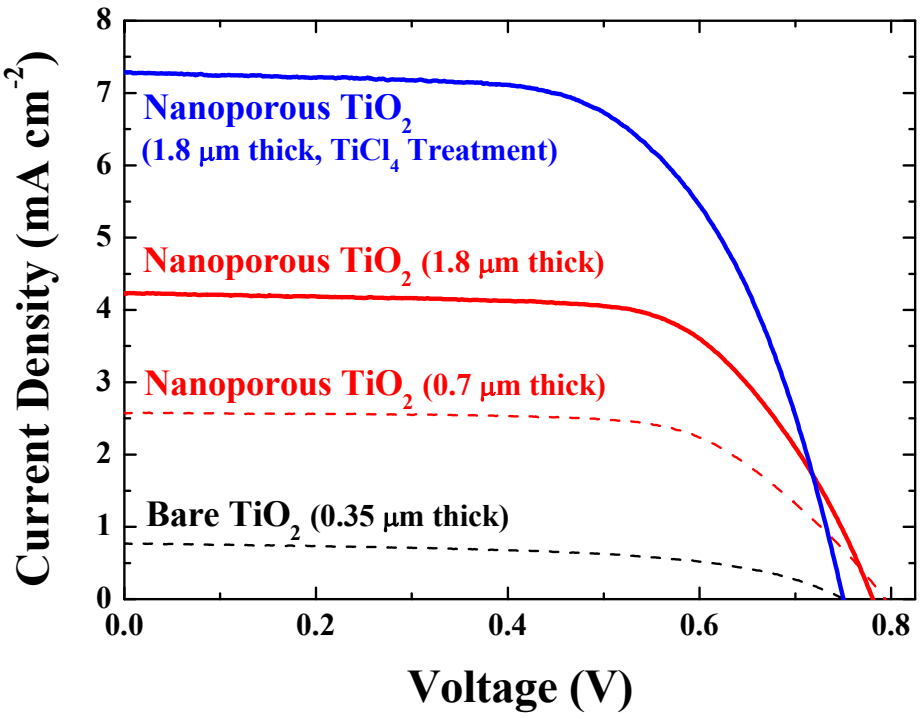

Fig. 3-8. (Color) Photocurrent density-voltage (*J-V*) characteristics of DSSCs.

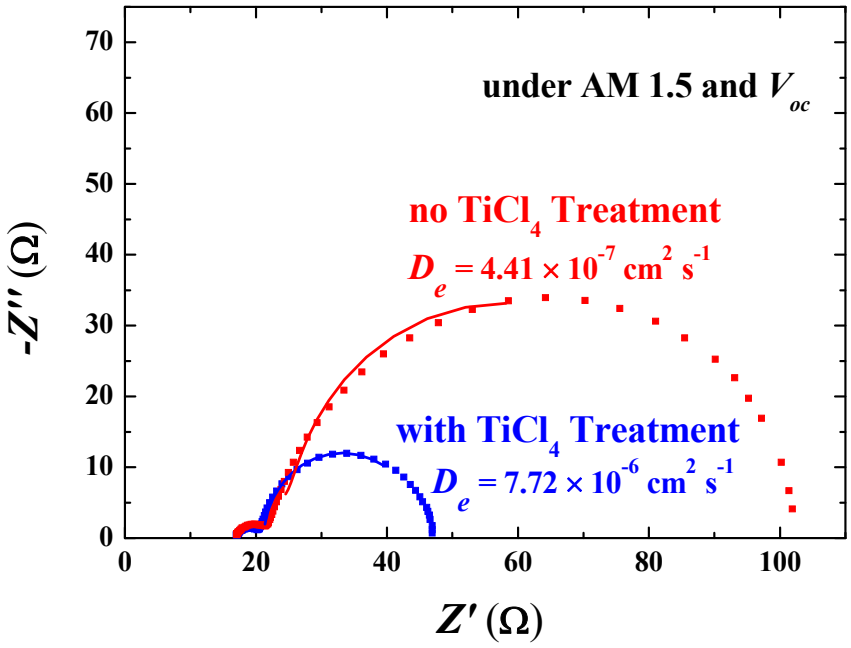

Fig. 3-9. (Color) Nyquist plots showing electrochemical impedance at open-circuit voltage (symbol), with the corresponding electron diffusivities (D_e) (from solid fitting line).

Table 3-2. Short-circuit current (J_{sc}), open-circuit voltage (V_{oc}), fill factor, and power-conversion efficiency (η) of thin-film TiO_2 DSSCs.

	J_{sc} (mA cm^{-2})	V_{oc} (V)	Fill Factor	η
Bare TiO_2 (0.35 μm thick)	**0.77**	**0.750**	**55.2%**	**0.32%**
Nanoporous TiO_2 (0.7 μm thick)	**2.58**	**0.793**	**66.2%**	**1.35%**
Nanoporous TiO_2 (1.8 μm thick)	**4.23**	**0.781**	**66.2%**	**2.19%**
$TiCl_4$-Treated Nanoporous TiO_2 (1.8 μm thick)	**7.29**	**0.750**	**62.7%**	**3.43%**

Since $(D_e\tau)^{1/2}$ in DSSCs is directly proportional to $(R_{rec}/R_{tr})^{1/2}$ (where R_{rec} and R_{tr} represent the electron-recombination and electron-transport resistance, respectively) [39,40], it is suggested that loss of photoelectrons via recombination reactions and slow photoelectron transport would be more dominant in the nanoporous-TiO_2 DSSC ($(D_e\tau)^{1/2}$ = 1.24 μm), compared with the typical nanoparticulate-TiO_2 films ($(D_e\tau)^{1/2}$ = several μm [35,41]). Shorter $(D_e\tau)^{1/2}$ and therefore defectiveness are attributed to the smaller pore size (Table 3-1) and more grain boundaries. Furthermore, oxygen vacancy, hydroxyl group, and five-fold coordinated Ti atom are known to act as recombination centers at the surface of TiO_2 [42,43], so passivation of these defects can increase R_{rec} and decrease R_{tr} at the same time.

Formation of additional sub-nm-thick TiO_2 layer by $TiCl_4$ treatment, which is widely used in the DSSC-field to increase η [33,44], is expected to alleviate various surface defects of our nanoporous-TiO_2 film. In addition, growth of TiO_2 nanocrystallites by the $TiCl_4$ treatment also improves the R_{rec}/R_{tr} ratio. Indeed, D_e of the nanoporous-TiO_2 film is enhanced by more than one order of magnitude through the $TiCl_4$ treatment (Fig. 3-9), and the corresponding $(D_e\tau)^{1/2}$ is improved to 3.21 μm. As a result, η_{cc} increases to 88% (from 54% before the $TiCl_4$ treatment), which means that photoelectron collection of nanoporous-TiO_2 DSSC is significantly improved by the $TiCl_4$ treatment. Electron lifetimes (τ) deduced from open-circuit voltage (V_{oc}) decays [45] also show the $TiCl_4$-treatment effects on the photoelectron-transport properties (Fig. 3-10).

With the $TiCl_4$ treatment, short-circuit current (J_{sc}) and η of the 1.8-μm-thick nanoporous-TiO_2 DSSC increased by 72% and 57%, respectively (Fig. 3-8, Fig. 3-11,

and Table 3-2), despite the reduced dye loading (Fig. 3-12). In the conventional nanoparticulate-TiO_2 DSSCs, increase of dye loading induced by enlarged actual surface area has been suggested as one of the enhancement mechanisms by the $TiCl_4$ treatment [33,44]. On the contrary, the $TiCl_4$ treatment shrinks the pores in the nanoporous-TiO_2 photoelectrode, and therefore both surface area and the amount of adsorbed dye decrease (Fig. 3-12). The *IPCE* at arbitrary wavelength λ can be expressed as [46]:

$$IPCE(\lambda) = LHE(\lambda) \cdot \varphi_{inj} \cdot \eta_{cc},$$

where $LHE(\lambda)$ is the light-harvesting efficiency, and φ_{inj} is the quantum yield for electron injection from dye to photoelectrode. The $TiCl_4$ treatment led to the enhancement of *IPCE* over the whole wavelength (Fig. 3-11) in spite of the decreased dye loading and thus lower *LHE* (Fig. 3-12), and these results qualitatively indicate that the increased photocurrent by the $TiCl_4$ treatment comes from the enhancement of η_{cc} ($\varphi_{inj} \sim 1$ for N719 dye-TiO_2 system [46]). Finally, power-conversion efficiency of 3.43% is attained with the 1.8-μm-thick nanoporous-TiO_2 thin film, and this value is much superior to that of DSSCs fabricated by the conventional TiO_2-nanoparticle method with similar thickness. (The average $\eta = 2.25\%$ at 1.5 μm [47] and $\eta = 1.08\%$ at 1.1 μm [48], without the $TiCl_4$ treatment. We consider that enhancement by the $TiCl_4$ treatment in the nanoparticulate-TiO_2 DSSCs is generally 10 - 20% [33,44].)

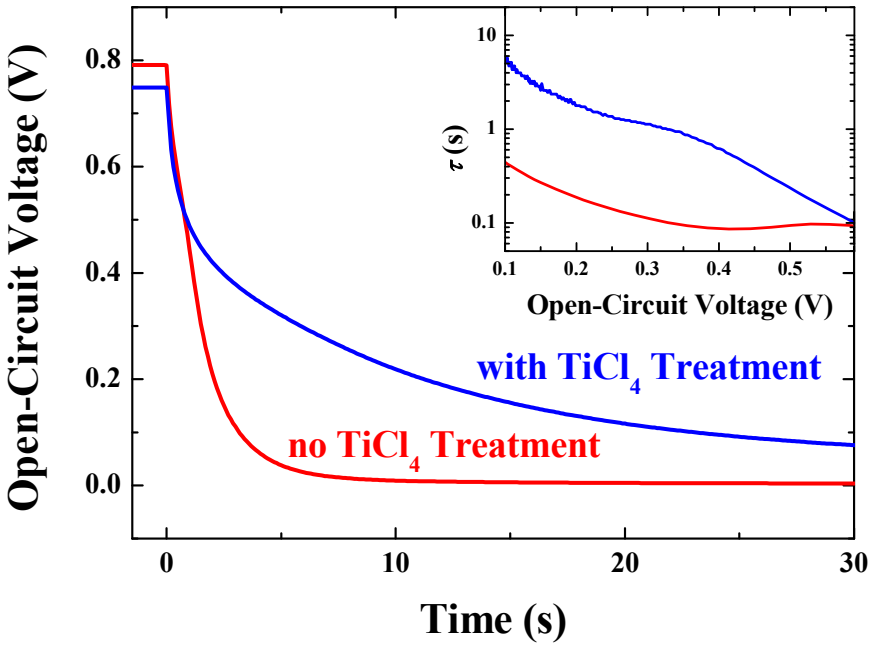

Fig. 3-10. (Color) V_{oc} decaying curves of DSSCs. The inset exhibits electron lifetimes (τ) in DSSCs, deduced from the V_{oc} decaying curves.

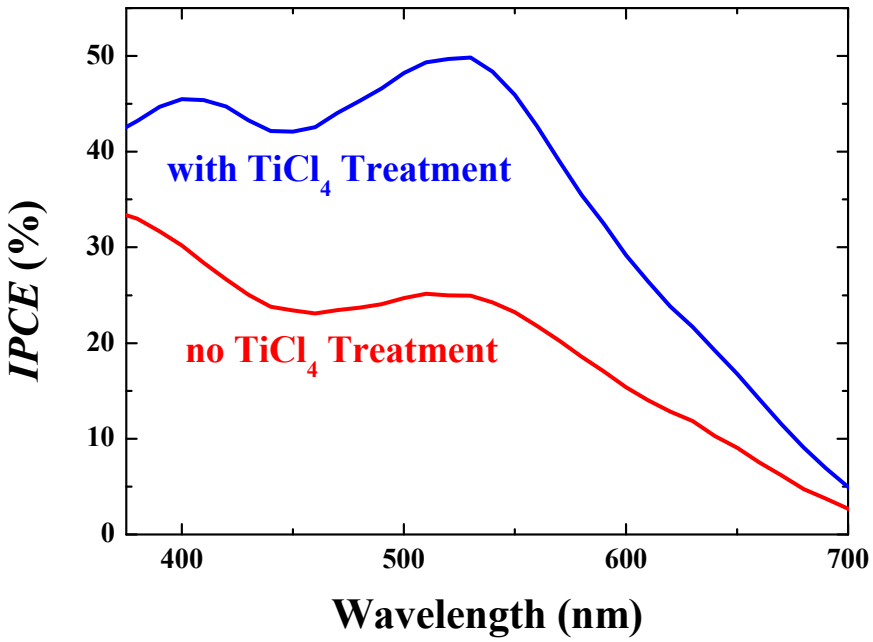

Fig. 3-11. (Color) Incident photon-to-current conversion efficiency (*IPCE*) spectra of nanoporous-TiO_2 DSSCs.

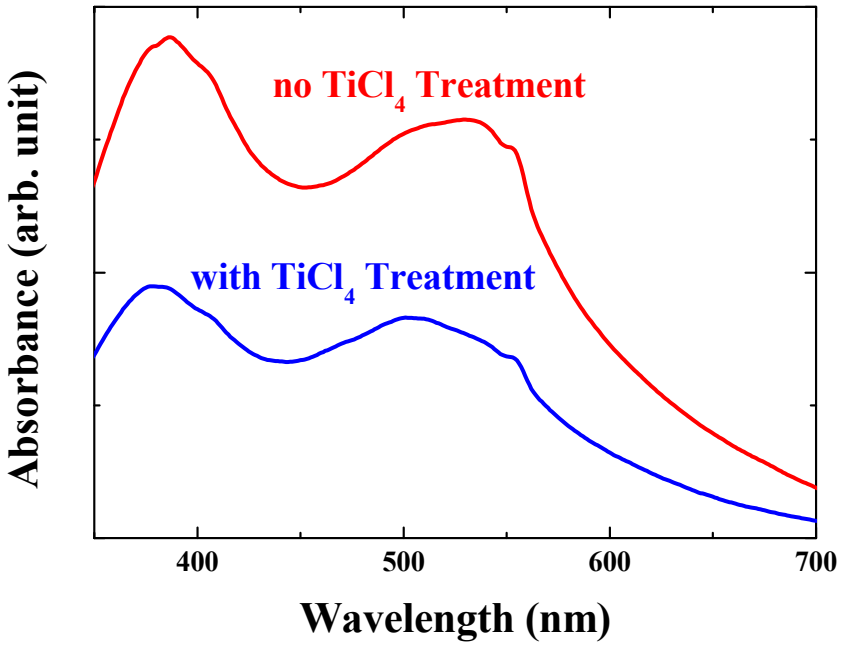

Fig. 3-12. (Color) Absorption spectra of desorbed dye solutions from $TiCl_4$-treated nanoporous-TiO_2 film (blue) and non-treated nanoporous-TiO_2 film (red).

3.4. Conclusions

We developed a straightforward and effective method to fabricate nanoporous-TiO_2 thin films using co-sputtering and selective etching. Our nanoporous-TiO_2 thin films were applied to the photoelectrode of DSSCs, and showed power-conversion efficiencies of up to 3.4% at the thickness of just 1.8 μm. The nanoporous-TiO_2 film exhibited porosity of ~63%, and this value is comparable to a typical nanoparticulate-TiO_2 film used in DSSCs. However, surface area of our nanoporous-TiO_2 film was calculated as ~230 m^2 g^{-1}, which is 3 times greater than that of the nanoparticulate-TiO_2 film. The $TiCl_4$ treatment on the nanoporous-TiO_2 photoelectrode led to the effective collection of photoelectrons, and thereby both photocurrent and power-conversion efficiency of the DSSC were enhanced in spite of the reduced dye loading. We expect that this technique can be utilized for large-scale deposition of photoelectrodes and mass production of sensitized solar cells. Furthermore, not limited to TiO_2 and sensitized solar cells, nanoporous thin films with various materials and diverse purposes can be fabricated through this facile technique.

3.5. References

1. A. Hagfeldt, G. Boschloo, L. Sun, L. Kloo, and H. Pettersson, "Dye-Sensitized Solar Cells," *Chem. Rev.* **110**, 6595 (2010).
2. S. Rühle, M. Shalom, and A. Zaban, "Quantum-Dot-Sensitized Solar Cells," *ChemPhysChem* **11**, 2290 (2010).
3. H. McDaniel, P. E. Heil, C.-L. Tsai, K. Kim, and M. Shim, "Integration of Type II Nanorod Heterostructures into Photovoltaics," *ACS Nano* **5**, 7677 (2011).
4. H. Choi, R. Nicolaescu, S. Paek, J. Ko, and P. V. Kamat, "Supersensitization of CdS Quantum Dots with a Near-Infrared Organic Dye: Toward the Design of Panchromatic Hybrid-Sensitized Solar Cells," *ACS Nano* **5**, 9238 (2011).
5. C.-H. Lin, S. Chattopadhyay, C.-W. Hsu, M.-H. Wu, W.-C. Chen, C.-T. Wu, S.-C. Tseng, J.-S. Hwang, J.-H. Lee, C.-W. Chen, C.-H. Chen, L.-C. Chen, and K.-H. Chen, "Enhanced Charge Separation by Sieve-Layer Mediation in High-Efficiency Inorganic-Organic Solar Cells," *Adv. Mater.* **21**, 759 (2009).
6. H. Zhang, X. Yu, and P. V. Braun, "Three-Dimensional Bicontinuous Ultrafast-Charge and -Discharge Bulk Battery Electrodes," *Nat. Nanotechnol.* **6**, 277 (2011).
7. J.-T. Jang, S. Jung, J.-W. Seo, M.-C. Kim, E. Sim, Y. Oh, S. Nam, B. Park, and J. Cheon, "Ultrathin Zirconium Disulfide Nanodiscs," *J. Am. Chem. Soc.* **133**, 7636 (2011).
8. Y. Park, B. Lee, C. Kim, J. Kim, S. Nam, Y. Oh, and B. Park, "Modification of Gold Catalysis with Aluminum Phosphate for Oxygen-Reduction Reaction," *J. Phys.*

Chem. C **114**, 3688 (2010).

9. C. Kim, B. Lee, Y. Park, B. Park, J. Lee, and H. Kim, "Iron-Phosphate/Platium/Carbon Nanocomposites for Enhanced Electrocatalytic Stability," *Appl. Phys. Lett.* **91**, 113101 (2007).
10. B. O'Regan and M. Grätzel, "A Low-Cost, High-Efficiency Solar Cell Based on Dye-Sensitized Colloidal TiO_2 Films, " *Nature* **353**, 737 (1991).
11. A. Yella, H.-W. Lee, H. N. Tsao, C. Yi, A. K. Chandiran, M. K. Nazeeruddin, E. W.-G. Diau, C.-Y. Yeh, S. M. Zakeerudding, and M. Grätzel, "Porphyrin-Sensitized Solar Cells with Cobalt (II/III)-Based Redox Electrolyte Exceed 12 Percent Efficiency," *Science* **334**, 629 (2011).
12. S. Ito, P. Chen, P. Comte, M. K. Nazeeruddin, P. Liska, P. Péchy, and M. Grätzel, "Fabrication of Screen-Printing Pastes from TiO_2 Powders for Dye-Sensitized Solar Cells," *Prog. Photovoltaics* **15**, 603 (2007).
13. M. K. Nazeeruddin, A. Kay, I. Rodicio, R. Humphry-Baker, E. Müller, P. Liska, N. Vlachopoulos, and M. Grätzel, "Conversion of Light to Electricity by *cis*-X_2Bis(2,2'-bipyridyl-4,4'-dicarboxylate)ruthenium(II) Charge-Transfer Sensitizers (X = Cl^-, Br^-, I^-, CN^-, and SCN^-) on Nanocrystalline TiO_2 Electrodes," *J. Am. Chem. Soc.* **115**, 6382 (1993).
14. B. Liu and E. S. Aydil, "Growth of Oriented Single-Crystalline Rutile TiO_2 Nanorods on Transparent Conducting Substrates for Dye-Sensitized Solar Cells," *J. Am. Chem. Soc.* **131**, 3985 (2009).
15. G. K. Mor, K. Shankar, M. Paulose, O. K. Varghese, and C. A. Grimes, "Use of

Highly-Ordered TiO_2 Nanotube Arrays in Dye-Sensitized Solar Cells," *Nano Lett.* **6**, 215 (2006).

16. J. Yan and F. Zhou, "TiO_2 Nanotubes: Structure Optimization for Solar Cells," *J. Mater. Chem.* **21**, 9406 (2011).
17. N. Tétreault and M. Grätzel, "Novel Nanostructures for Next Generation Dye-Sensitized Solar Cells," *Energy Environ. Sci.* **5**, 8506 (2012).
18. Y. G. Seo, K. Woo, J. Kim, H. Lee, and W. Lee, "Rapid Fabrication of an Inverse Opal TiO_2 Photoelectrode for DSSC Using a Binary Mixture of TiO_2 Nanoparticles and Polymer Microspheres," *Adv. Funct. Mater* **21**, 3094 (2011).
19. S.-C. Yang, D.-J. Yang, J. Kim, J.-M. Hong, H.-G. Kim, I.-D. Kim, and H. Lee, "Hollow TiO_2 Hemispheres Obtained by Colloidal Templating for Application in Dye-Sensitized Solar Cells," *Adv. Mater.* **20**, 1059 (2008).
20. D. Kim, K. Lee, P. Roy, B. I. Birajdar, E. Spiecker, and P. Schmuki, "Formation of a Non-Thickness-Limited Titanium Dioxide Mesosponge and its Use in Dye-Sensitized Solar Cells," *Angew. Chem. Int. Ed.* **48**, 9326 (2009).
21. P. J. Kelly and R. D. Arnell, "Magnetron Sputtering: a Review of Recent Developments and Applications," *Vacuum* **56**, 159 (2000).
22. M. M. Gómez, J. Lu, J. L. Solis, E. Olsson, A. Hagfeldt, and C. G. Granqvist, "Dye-Sensitized Nanocrystalline Titanium-Oxide-Based Solar Cells Prepared by Sputtering: Influence of the Substrate Temperature during Deposition," *J. Phys. Chem. B* **104**, 8712 (2000).
23. M. F. Hossain, S. Biswas, T. Takahashi, Y. Kubota, and A. Fujishima, "Investigation

of Sputter-Deposited TiO_2 Thin Film for the Fabrication of Dye-Sensitized Solar Cells," *Thin Solid Films* **516**, 7149 (2008).

24. J. Erlebacher, M. J. Aziz, A. Karma, N. Dimitrov, and K. Sieradzki, "Evolution of Nanoporosity in Dealloying," *Nature* **410**, 450 (2001).
25. J. C. Thorp, K. Sieradzki, L. Tang, P. A. Crozier, A. Misra, M. Nastasi, D. Mitlin, and S. T. Picraux, "Formation of N anoporous Noble Metal Thin Films by Electrochemical Dealloying of Pt_xSi_{1-x}," *Appl. Phys. Lett.* **88**, 033110 (2006).
26. Y. Oh, J. Kang, S. Nam, S. Byun, and B. Park, "Pt/$AlPO_4$ Nanocomposite Thin-Film Electrodes for Ethanol Electrooxidation," *Mater. Chem. Phys.* **135**, 188 (2012).
27. B. Lee, C. Kim, Y. Park, T.-G. Kim, and B. Park, "Nanostructured Platinum/Iron-Phosphate Thin-Film Electrodes for Methanol Oxidation," *Electrochem. Solid-State Lett.* **9**, E27 (2006).
28. S. J. Yoo, T.-Y. Jeon, Y.-H. Cho, K.-S. Lee, and Y.-E. Sung, "Particle Size Effects of PtRu Nanoparticles Embedded in TiO_2 on Methanol Electrooxidation," *Electrochim. Acta* **55**, 7939 (2010).
29. J. W. Lim, S. J. Yoo, S. H. Park, S. U. Yun, and Y.-E. Sung, "High Electrochromic Performance of co-Sputtered Vanadium-Titanium Oxide as a Counter Electrode," *Sol. Energy Mater. Sol. Cells* **93**, 2069 (2009).
30. A. Rupérez and J. J. Laserna, "Surface-Enhanced Raman Spectrometry on a Silver Substrate Prepared by the Nitric Acid Etching Method," *Anal. Chim. Acta* **291**, 147 (1994).
31. D.-R. Jung, D. Son, J. Kim, C. Kim, and B. Park, "Highly-Luminescent Surface-

Passivated ZnS:Mn Nanoparticles by a Simple One-Step Synthesis" *Appl. Phys. Lett.* **93**, 163118 (2008).

32. D. Son, D.-R. Jung, J. Kim, T. Moon, C. Kim, and B. Park, "Synthesis and Photoluminescence of Mn-Doped Zinc Sulfide Nanoparticles" *Appl. Phys. Lett.* **90**, 101910 (2007).
33. S. Ito, P. Liska, P. Comte, R. Charvet, P. Péchy, Udo Bach, L. Schmidt-Mende, S. M. Zakeeruddin, A. Kay, M. K. Nazeeruddin, and M. Grätzel, "Control of Dark Current in Photoelectrochemical (TiO_2/I^--I_3^-) and Dye-Sensitized Solar Cells," *Chem. Commun.* 4351 (2005).
34. C. J. Barbé, F. Arendse, P. Comte, M. Jirousek, F. Lenzmann, V. Shklover, and M. Grätzel, "Nanocrystalline Titanium Oxide Electrodes for Photovoltaic Applications," *J. Am. Ceram. Soc.* **80**, 3157 (1997).
35. M. Adachi, M. Sakamoto, J. Jiu, Y. Ogata, and S. Isoda, "Determination of Parameters of Electron Transport in Dye-Sensitized Solar Cells Using Electrochemical Impedance Spectroscopy," *J. Phys. Chem. B* **110**, 13872 (2006).
36. S. Kambe, S. Nakade, Y. Wada, T. Kitamura, and S. Yanagida, "Effects of Crystal Structure, Size, Shape and Surface Structural Differences on Photo-Induced Electron Transport in TiO_2 Mesoporous Electrodes," *J. Mater. Chem.* **12**, 723 (2002).
37. R. Kern, R. Sastrawan, J. Ferber, R. Stangl, and J. Luther, "Modeling and Interpretation of Electrical Impedance Spectra of Dye Solar Cells Operated under Open-Circuit Conditions," *Electrochim. Acta* **47**, 4213 (2002).
38. J. van de Lagemaat, N.-G. Park, and A. J. Frank, "Influence of Electrical Potential

Distribution, Charge Transport, and Recombination on the Photopotential and Photocurrent Conversion Efficiency of Dye-Sensitized Nanocrystalline TiO_2 Solar Cells: A Study by Electrical Impedance and Optical Modulation Techniques," *J. Phys. Chem. B* **104**, 2044 (2000).

39. J. Bisquert, "Theory of the Impedance of Electron Diffusion and Recombination in a Thin Layer," *J. Phys. Chem. B* **106**, 325 (2002).
40. F. Fabregat-Santiago, G. Garcia-Belmonte, I. Mora-Seró, and J. Bisquert, "Characterization of Nanostructured Hybrid and Organic Solar Cells by Impedance Spectroscopy," *Phys. Chem. Chem. Phys.* **13**, 9083 (2011).
41. P. R. F. Barnes, A. Y. Anderson, S. E. Koops, J. R. Durrant, and B. C. O'Regan, "Electron Injection Efficiency and Diffusion Length in Dye-Sensitized Solar Cells Derived from Incident Photon Conversion Efficiency Measurements," *J. Phys. Chem. C* **113**, 1126 (2009).
42. S. Wendt, P. T. Sprunger, E. Lira, G. K. H. Madsen, Z. Li, J. Ø. Hansen, J. Matthiesen, A. Blekinge-Rasmussen, E. Lægsgaard, B. Hammer, and F. Besenbacher, "The Role of Interstitial Sites in the Ti*3d* Defect State in the Band Gap of Titania," *Science* **320**, 1755 (2008).
43. S. M. Prokes, J. L. Gole, X. B. Chen, C. Burda, and W. E. Carlos, "Defect-Related Optical Behavior in Surface Modified TiO_2 Nanostructures," *Adv. Funct. Mater.* **15**, 161 (2005).
44. P. M. Sommeling, B. C. O'Regan, R. R. Haswell, H. J. P. Smit, N. J. Bakker, J. J. T. Smits, J. M. Kroon, and J. A. M. van Roosmalen, "Influence of a $TiCl_4$ Post-

Treatment on Nanocrystalline TiO_2 Films in Dye-Sensitized Solar Cells," *J. Phys. Chem. B* **110**, 19191 (2006).

45. A. Zaban, M. Greenshtein, and J. Bisquert, "Determination of the Electron Lifetime in Nanocrystalline Dye Solar Cells by Open-Circuit Voltage Decay Measurements," *ChemPhysChem* **4**, 859 (2003).
46. M. Grätzel, "Solar Energy Conversion by Dye-Sensitized Photovoltaic Cells," *Inorg. Chem.* **44**, 6841 (2005).
47. J. Qi, X. Dang, P. T. Hammond, and A. M. Belcher, "Highly Efficient Plasmon-Enhanced Dye-Sensitized Solar Cells through Metal@Oxide Core-Shell Nanostructure," *ACS Nano* **5**, 7108 (2011).
48. M. D. Brown, T. Suteewong, R. S. S. Kumar, V. D'Innocenzo, A. Petrozza, M. Lee, U. Wiesner, and H. J. Snaith, "Plasmonic Dye-Sensitized Solar Cells Using Core-Shell Metal-Insulator Nanoparticles," *Nano Lett.* **11**, 438 (2011).

Appendix: List of Publications and Presentations

A.1. Publications (International):

1. **Changwoo Nahm**, Hongsik Choi, Jongmin Kim, Dae-Ryong Jung, Chohui Kim, Joonhee Moon, Byungjoo Lee, and Byungwoo Park, "The Effects of 100 nm-Diameter Au Nanoparticles on Dye-Sensitized Solar Cells," *Appl. Phys. Lett.* **99**, 253107 (2011).
2. **Changwoo Nahm**,[+] Dae-Ryong Jung,[+] Jongmin Kim, Seunghoon Nam, Hongsik Choi, Saeromi Hong, Taehyun Hwang, Taeho Moon, and Byungwoo Park, "Photoluminescence Enhancement by Surface-Plasmon Resonance: Recombination-Rate Theory and Experiments," *Appl. Phys. Express* **6**, 052001 (2013).
3. **Changwoo Nahm**,[+] Sungjin Shin,[+] Woojin Lee, Jae Ik Kim, Dae-Ryong Jung, Jongmin Kim, Seunghoon Nam, Sujin Byun, and Byungwoo Park, "Electronic Transport and Carrier Concentration in Conductive ZnO:Ga Thin Films," *Curr. Appl. Phys.* **13**, 415 (2013).
4. **Changwoo Nahm**,[+] Chunjoong Kim,[+] Yejun Park, and Byungwoo Park, "Nanoporous Pt Thin Films with Superior Catalytic Activities by the Electrochemical Dissolution of Al," *Met. Mater. Inter.* **15**, 989 (2009).
5. **Changwoo Nahm**, Chunjoong Kim, Yejun Park, Byungjoo Lee, and Byungwoo Park, "Iron-Phosphate/Pt Nanostructured Electrodes for High-Efficiency Fuel Cells," *Electron. Mater. Lett.* **4**, 5 (2008).
6. Hongsik Choi, **Changwoo Nahm**, Jongmin Kim, Joonhee Moon, Seunghoon Nam, Chohui Kim, Dae-Ryong Jung, and Byungwoo Park, "The Effect of $TiCl_4$-Treated TiO_2 Compact Layer on the Performance of Dye-Sensitized Solar Cell," *Curr. Appl. Phys.* 12, 737 (2012).

7. Jongmin Kim, Hongsik Choi, **Changwoo Nahm**, Chohui Kim, Jae Ik Kim, Woojin Lee, Suji Kang, Byungho Lee, Taehyun Hwang, Helen Hejin Park, and Byungwoo Park, "Graded Bandgap Structure for PbS/CdS/ZnS Quantum-Dot-Sensitized Solar Cells with a $Pb_xCd_{1-x}S$ Interlayer," *Appl. Phys. Lett.* **102**, 183901 (2013).

8. Jongmin Kim, Hongsik Choi, **Changwoo Nahm**, Chohui Kim, Seunghoon Nam, Suji Kang, Dae-Ryong Jung, Jae Ik Kim, Joonhyeon Kang, and Byungwoo Park, "The Role of a $TiCl_4$ Treatment on the Performance of CdS Quantum-Dot-Sensitized Solar Cells," *J. Power Sources* (2012).

9. Seung-Yoon Lee, Woojin Lee, **Changwoo Nahm**, Jongmin Kim, Sujin Byun, Taehyun Hwang, Byung-Gi Lee, Young Il Jang, Sungeun Lee, Heon-Min Lee, and Byungwoo Park, "Nanostructural Analysis of ZnO:Al Thin Films for Carrier-Transport Mechanisms," *Curr. Appl. Phys.* **13**, 775 (2013).

10. Jongmin Kim,[+] Hongsik Choi,[+] **Changwoo Nahm**,[+] and Byungwoo Park, "Review Paper: Surface Plasmon Resonance for Photoluminescence and Solar-Cell Applications," *Electron. Mater. Lett.* (2012).

11. Seunghoon Nam, Sungun Wi, **Changwoo Nahm**, Hongsik Choi, and Byungwoo Park, "Challenges in Synthesizing Carbon-Coated $LiFePO_4$ Nanoparticles from Hydrous $FePO_4$ and Their Electrochemical Properties," *Mater. Res. Bull.* (2012).

12. Dae-Ryong Jung, Jongmin Kim, **Changwoo Nahm**, Seunghoon Nam, Jae Ik Kim, and Byungwoo Park, "Surface-Plasmon-Enhanced Photoluminescence of CdS Nanoparticles with Au/SiO_2 Nanocomposites," *Mater. Res. Bull.* **47**, 453 (2012).

13. Jongmin Kim, Hongsik Choi, **Changwoo Nahm**, Joonhee Moon, Chohui Kim, Seunghoon Nam, Dae-Ryong Jung, and Byungwoo Park, "The Effect of a Blocking Layer on the Photovoltaic Performance in CdS Quantum-Dot-Sensitized Solar Cells," *J. Power Sources* **196**, 10526 (2011).

14. Dae-Ryong Jung, Jongmin Kim, **Changwoo Nahm**, Hongsik Choi, Seunghoon

Nam, and Byungwoo Park, “Review Paper: Semiconductor Nanoparticles with Surface Passivation and Surface Plasmon,” *Electron. Mater. Lett.* **7**, 185 (2011).

15. Chunjoong Kim, Yejun Park, **Changwoo Nahm**, and Byungwoo Park, “Formation of Nanoporous Pt Thin Films by Electrochemical Dissolution,” *Electron. Mater. Lett.* **4**, 75 (2008).
16. Chohui Kim, Jongmin Kim, Hongsik Choi, **Changwoo Nahm**, Suji Kang, Sungjun Lee, Byungho Lee, and Byungwoo Park, “The Effect of TiO2-Coating Layer on the Performance in Nanoporous ZnO-Based Dye-Sensitized Solar Cells,” *J. Power Sources* **232**, 159 (2013).
17. Jae Ik Kim, Dae-Ryong Jung, Jongmin Kim, **Changwoo Nahm**, Sujin Byun, Sungjun Lee, and Byungwoo Park, “Surface-Plasmon-Coupled Photoluminescence from CdS Nanoparticles with Au Films,” *Soild State Commun.* **152**, 1767 (2012).
18. Dae-Ryong Jung, Jongmin Kim, Seunghoon Nam, **Changwoo Nahm**, Hongsik Choi, Jae Ik Kim, Junhee Lee, Chohui Kim, and Byungwoo Park, “Photoluminescence Enhancement in CdS Nanoparticles by Surface-Plasmon Resonance,” *Appl. Phys. Lett.* **99**, 041906 (2011).
19. Woojin Lee, Hoechang Kim, Dae-Ryong Jung, Jongmin Kim, **Changwoo Nahm**, Junhee Lee, Suji Kang, Byungho Lee, and Byungwoo Park, “An Effective Oxidation Approach for Luminescence Enhancement in CdS Quantum Dots by H_2O_2,” *Nanoscale. Res. Lett.* **7**, 672 (2012).
20. Woojin Lee, Sungjin Shin, Dae-Ryong Jung, Jongmin Kim, **Changwoo Nahm**, Taeho Moon, and Byungwoo Park, “Investigation of Electronic and Optical Properties in Al-Ga Codoped ZnO Thin Films,” *Curr. Appl. Phys.* **12**, 628 (2012).

A.2. Presentations (International):

1. **Changwoo Nahm**, Hongsik Choi, Jongmin Kim, and Byungwoo Park, "Simple 'Deposition and Selective Etching' Process for Nanoporous TiO_2 Thin Film and Its Application to Dye-Sensitized Solar Cells," *Global Photovoltaic Conference 2012 (GPVC 2012)*, Busan, Korea, November 2012.
   [Poster by C. Nahm]

2. **Changwoo Nahm**, Hongsik Choi, Jongmin Kim, and Byungwoo Park, "Simple 'Deposition and Selective Etching' Process for Nanoporous TiO_2 Thin Film and Its Application to Dye-Sensitized Solar Cells," *The 13th Korea-Japan Student Symposium (Seoul National University - Tohoku University)*, Seoul, Korea, November 2012.
   [Poster by C. Nahm]

3. **Changwoo Nahm**, Hongsik Choi, Jongmin Kim, Dae-Ryong Jung, Chohui Kim, and Byungwoo Park, "The Effects of 100 nm-Diameter Au Nanoparticles on Dye-Sensitized Solar Cells," *Materials Research Society (MRS) Fall Meeting*, Boston, MA, November 2011.
   [Oral by C. Nahm]

4. **Changwoo Nahm**, Chunjoong Kim, Yejun Park, and Byungwoo Park, "Nanoscale Control of Pt-Based Electrodes," *Materials Research Society (MRS) Fall Meeting*, Boston, MA, December 2009.
   [Oral by C. Nahm]

5. **Changwoo Nahm**, Chunjoong Kim, Yejun Park, and Byungwoo Park, "Nanoporous Pt Thin Films with Enhanced Catalytic Activities by Electrochemical Dissolution of Al," *The 9th Korea - Japan Student Symposium (Seoul National University - Tohoku University)*, Seoul, Korea, November 20-22, 2008.
   [Oral by C. Nahm]

6. Chunjoong Kim, Yejun Park, **Changwoo Nahm**, and Byungwoo Park, "Nanoporous Pt Thin Films with Superior Catalytic Activities by the Electrochemical Dissolution of Al," *The 3rd Seoul National University - University of Tokyo - Tsinghua University Joint Student Workshop*, Seoul, Korea, October 2007.
   [Poster by C. Nahm]

7. Byungwoo Park, Jongmin Kim, **Changwoo Nahm**, Hongsik Choi, Seunghoon Nam, and Chohui Kim, "Semiconductor Nanoparticles with Surface Passivation and Surface Plasmon for Luminescence and Solar-Cell Applications," *Materials Science & Technology 2012 (MS&T'12)*, Pittsburgh, PA, October 7-11, 2012.

8. Dae-Ryong Jung, Jongmin Kim, Seunghoon Nam, **Changwoo Nahm**, Hongsik Choi, Jae Ik Kim, Junhee Lee, Chohui Kim, and Byungwoo Park, "Photoluminescence Enhancement in CdS Nanoparticles by Surface-Plasmon Resonance," *Materials Research Society (MRS) Fall Meeting*, Boston, MA, November 2011.

9. Jongmin Kim, Hongsik Choi, **Changwoo Nahm**, Joonhee Moon, Chohui Kim, Seunghoon Nam, Dae-Ryong Jung, and Byungwoo Park, "The Effect of a Blocking Layer on the Photovoltaic Performance in CdS Quantum-Dot-Sensitized Solar Cells," *Materials Research Society (MRS) Fall Meeting*, Boston, MA, November 2011.

10. Hongsik Choi, **Changwoo Nahm**, Jongmin Kim, Joonhee Moon, Seunghoon Nam, Chohui Kim, Dae-Ryong Jung, and Byungwoo Park, "The Effect of $TiCl_4$-Treated TiO_2 Compact Layer on the Performance of Dye-Sensitized Solar Cell," *Materials Research Society (MRS) Fall Meeting*, Boston, MA, November 2011.

11. Chohui Kim, Jongmin Kim, Hongsik Choi, **Changwoo Nahm**, and Byungwoo Park, "Suppression of Charge Recombination in Photoelectrodes of TiO_2-Coated ZnO Aggregates Using Wet-Chemical Processing," *Materials Research Society (MRS)*

Fall Meeting, Boston, MA, November 2011.

12. Byungwoo Park, Dae-Ryong Jung, Jongmin Kim, **Changwoo Nahm**, Hongsik Choi, and Seunghoon Nam, "Semiconductor Nanoparticles with Surface Passivation and Surface Plasmon," *International Union of MRS (IUMRS)*, Taipei, Taiwan, September 2011.

13. Byungwoo Park, Yejun Park, Yuhong Oh, Jongmin Kim, **Changwoo Nahm**, and Seunghoon Nam, "Nanomaterials for Electrodes in Rechargeable Battery and Fuel Cell," *Materials Research Society (MRS) Spring Meeting*, San Francisco, CA, April 2010.

14. Byungwoo Park, Yejun Park, Yuhong Oh, Jongmin Kim, **Changwoo Nahm**, and Seunghoon Nam, "Nanomaterials for Electrodes in Rechargeable Battery and Fuel Cell," *The Forth Asian Conference on Electrochemical Power Sources (ACEPS-4)*, National Taiwan University, Taipei, Taiwan, November 8-12, 2009.

15. Chunjoong Kim, Yejun Park, **Changwoo Nahm**, and Byungwoo Park, "Nanostructured Pt-Based Electrodes for the Enhanced Electrocatalytic Activities," *Materials Research Society (MRS) Fall Meeting*, Boston, MA, December 2008.

16. Chunjoong Kim, **Changwoo Nahm**, Yejun Park, and Byungwoo Park, "Nanoporous Pt Thin Films with Superior Catalytic Activities by the Electrochemical Dissolution of Al," *Materials Research Society (MRS) Spring Meeting*, San Francisco, CA, March 2008.

17. Byungwoo Park, Joon-Gon Lee, Donggi Ahn, Chunjoong Kim, Yejun Park, Yuhong Oh, and **Changwoo Nahm**, "Nanoscale Interface Control of High-Quality Electrode Materials for Li-Ion Battery and Fuel Cell," *The Second Asian Conference on Electrochemical Power Sources (ACEPS-2)*, Fudan University, Shanghai, China, October 22, 2007.

국문 초록

염료감응형 태양전지는 10% 이상의 광전변환효율을 나타내는 효율적인 광전기화학시스템이지만, 지난 20 여년간의 연구를 통해 재료 및 소자제작기술이 최적화되어 소자의 효율은 한계점에 다다른 상태이다. 염료감응형 태양전지의 산업화 및 상용화를 위해서는 소자의 광전변환효율 향상 뿐만 아니라 대량생산을 위한 차세대 공정 개발이 필요하며, 이를 위해 재료·화학·물리 등 다양한 분야에서 심도깊은 연구가 진행되고 있다.

본 학위논문은, 염료감응형 태양전지 광전극의 나노구조를 조절하여 소자의 광전변환효율을 향상시킨 연구 내용에 대하여 보고하고 있다. 금속나노구조에서 발생하는 표면플라즈몬현상을 적용하여 광전극의 광학적 특성을 조절하고 이를 통한 소자의 광흡수·광전류 변화를 관찰하였으며, 스퍼터링증착 및 선택적용해 방법을 통해 염료감응형 태양전지 광전극용 나노다공성 이산화티타늄 박막을 제작하는 새로운 공정을 제시하였다. 또한 광전극의 광학적/나노구조적 특성과 태양전지의 광변환특성 사이의 상관관계에 대해서도 면밀하게 분석하였다.

본 학위논문의 1 장은 염료감응형 태양전지에 대한 소개로 시작하고 있다. 염료감응형 태양전지의 작동 원리, 구성 요소, 그리고 사용되는 재료에 대한 설명이 수록되어 있으며, 특히 광전극 재료로 사용되는 산화물나노구조에 대한 다양한 선행연구에 대해 자세히 설명하고 있다. 또한 금속나노구조에서 발생하는 표면플라즈몬 현상 및 이를 이용한 태양전지의 광흡수 및 광전류 향상 가능성에 대해서도 설명하고 있다.

2 장에서는, 이산화티타늄 나노입자광전극에 100 나노미터 크기의 금 나노입자를 첨가한 연구 결과에 대해 보고하고 있다. 최적 조건에서 광전변환효율은 2.7%에서 3.3%로 향상되었으며, 광전류 향상이 소자의 효율

향상으로 이어졌다. 광흡수 측정을 통해, 광전극 내부의 금 나노입자는 표면플라즈몬을 통해 빛을 강하게 흡수하고 소자의 광흡수를 증가시킨다는 것을 확인하였으며, 표면플라즈몬에 의해 금 나노입자 주변에서 전기장의 세기가 강해져 빛이 집중되고 이로 인해 광전류 생성이 향상된다는 메커니즘을 제시하였다.

3 장에서는 스퍼터링증착 및 선택적 용해를 통해 나노다공성 박막을 제작한 연구 결과에 대해 보고하고 있다. 스퍼터링 방법을 통해 은과 이산화티타늄을 동시증착하면, 은 나노클러스터와 이를 둘러싼 이산화티타늄 매트릭스로 구성된 나노복합체 박막이 만들어지고, 이 박막을 질산에 담가 은을 선택적으로 녹여내면 나노다공성 이산화티타늄 박막이 만들어진다. 이렇게 만들어진 나노다공성 이산화티타늄 박막을 염료감응형 태양전지 광전극으로 적용했을 때, 1.8 μm 의 얇은 두께에서 우수한 광전변환효율 3.4%가 보고되었다.

주요어: 염료감응형 태양전지, 표면플라즈몬, 나노다공성, 스퍼터링, 태양전지, 이산화티타늄

학번: 2009-30150